

# 1 Seeing the future: predictive control in neural models of ocular 2 accommodation

3  
4 Jenny C. A. Read<sup>1</sup>, Christos Kaspiris-Rousellis<sup>1</sup>, Toby S. Wood<sup>2</sup>, Bing Wu<sup>3</sup>, Björn N.S.  
5 Vlaskamp<sup>3</sup>, Clifton M. Schor<sup>4</sup>

6 1. Biosciences Institute, Newcastle University, NE2 4HH

7 2. School of Mathematics, Statistics & Physics, Newcastle University, NE1 7RU

8 3. Quantified Experience, Magic Leap Inc

9 4. School of Optometry, University of California at Berkeley

## 10 11 Abstract

12 Ocular accommodation is the process of adjusting the eye's crystalline lens so as to bring the  
13 retinal image into sharp focus. The major stimulus to accommodation is therefore retinal  
14 defocus, and in essence, the job of accommodative control is to send a signal to the ciliary  
15 muscle which will minimise the magnitude of defocus. In this paper, we first provide a tutorial  
16 introduction to control theory to aid vision scientists without this background. We then present  
17 a unified model of accommodative control that explains properties of the accommodative  
18 response for a wide range of accommodative stimuli. Following previous work, we conclude  
19 that most aspects of accommodation are well explained by dual integral control, with a "fast"  
20 or "phasic" integrator enabling response to rapid changes in demand, which hands over control  
21 to a "slow" or "tonic" integrator which maintains the response to steady demand. Control is  
22 complicated by the sensorimotor latencies within the system, which delay both information  
23 about defocus and the accommodation changes made in response, and by the sluggish response  
24 of the motor plant. These can be overcome by incorporating a Smith predictor, whereby the  
25 system predicts the delayed sensory consequences of its own motor actions. For the first time,  
26 we show that critically-damped dual integral control with a Smith predictor accounts for  
27 adaptation effects as well as for the gain and phase for sinusoidal oscillations in demand. In  
28 addition, we propose a novel proportional-control signal to account for the power spectrum of  
29 accommodative microfluctuations during steady fixation, which may be important in hunting  
30 for optimal focus, and for the nonlinear resonance observed for low-amplitude, high-frequency  
31 input. Complete Matlab/Simulink code implementing the model is provided at  
32 <https://doi.org/10.25405/data.ncl.14945550>.

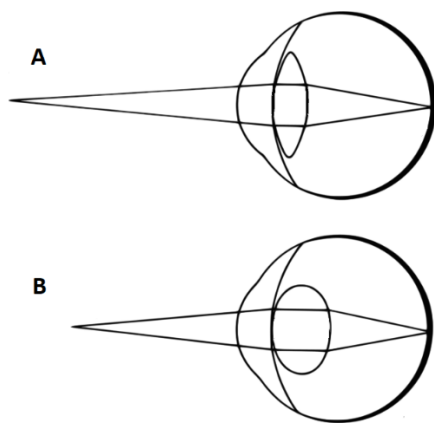
33

## 34 Introduction

35 Accommodation refers to the ability of the eye to change its focus between near and far  
36 distances, so as to ensure that images remain in sharp focus at the fovea across a wide range of  
37 object distances. This is achieved by changes in the convexity of the intra-ocular lens, brought  
38 about by contraction of the ciliary muscle (Figure 1). To focus on distant objects, the ciliary  
39 muscle is relaxed, the lens curvature and thus its optical power is minimal; to focus on near  
40 objects, the ciliary muscle contracts, the lens curvature increases and so does its optical power.  
41 Accommodation is usually controlled by the brain as an unconscious reflexive process.

42

43



44

45 *Figure 1. (A) Accommodating on a distant object. When the ciliary muscle is slack, tension in the suspensory zonules is released*  
46 *and the intra-ocular crystalline lens flattens, enabling distant objects to appear in focus on the retina (for an emmetropic*  
47 *eye). Light from a nearby object, such as shown, is therefore out of focus. (B) Accommodating on a nearby object. The ciliary*  
48 *muscle has contracted, increasing the curvature of the lens (blue arrows) in order to bring nearby objects into focus. Not to*  
49 *scale. Image: Pearson Scott Foresman, public domain.*

50

51 A full understanding of this process requires a knowledge of (i) the optical and biomechanical  
52 properties of the eye; (ii) how the required accommodative response is derived from retinal and  
53 extra-retinal cues; and (iii) the neural signals controlling the ciliary muscle to bring about this  
54 response. In this paper, we concentrate on the third of these.

55

56 In Section 1, we discuss the basic structure of models of neural control of accommodation. A  
57 key goal of this section is to provide a clear review of the subject, introducing concepts and  
58 summarizing previous work in a way which is accessible to vision scientists without a

59 background in classical control theory. Accordingly, this section acts as a tutorial to bring such  
60 readers up to speed.

61

62 The core of accommodative control is a negative feedback loop attempting to null the error  
63 between accommodative demand, i.e. the accommodation at which the fixated object will be  
64 in sharp focus, and response, i.e. the accommodation actually adopted. We introduce the Smith  
65 predictor (Miall et al., 1993; Smith, 1957), which incorporates a forward model of the motor  
66 plant to predict the eye's response to a motor command (and which might, in principle, also try  
67 to extrapolate the future sensory demand, though our model will not). Predictive models stand  
68 in contrast to models which do not take account of the sensory consequences of the body's own  
69 motor actions, and which are thus vulnerable to instabilities caused by the finite latencies within  
70 the control system.

71

72 Armed with this background, in Section 2 we discuss the evidence that accommodation uses a  
73 Smith predictor, and examine empirical constraints on the model parameters. We aim to  
74 produce a model which can account for behavior in both steady-state and smooth tracking,  
75 including accommodative lag/lead, adaptation, critical damping, and Bode plots of gain and  
76 phase. (Extending the model to reproduce dynamics of the step response (Bharadwaj & Schor,  
77 2005, 2006; Schor & Bharadwaj, 2006, 2004) will be covered in a subsequent paper.)

78

79 This analysis leads us to conclude that accommodative control most likely incorporates a  
80 predictor, in order to avoid instabilities due to the sensorimotor latency. Again, by “predictor”,  
81 we mean a forward model to predict the effect of commanded accommodation changes on the  
82 visual input, not necessarily anything that predicts changes in accommodative demand.

83

84 An oft-neglected component of accommodation models is the effect of noise in both closed-  
85 loop and open-loop mode. Noise is manifest as small ( $\sim 0.25D$ ) microfluctuations in the steady-  
86 state response (Campbell et al., 1959a; Kotulak & Schor, 1986b). We include a noise source,  
87 modelled as Gaussian noise added to the defocus signal. The presence of noise adds a further  
88 important constraint on model design. Predictive models have an internal feedback loop via a  
89 virtual plant as well as an external feedback loop via the ocular plant. Thus they can end up  
90 amplifying internal noise when run in open-loop mode. This is not observed empirically; in  
91 fact, the power spectrum of accommodation tends to show resonances in closed-loop rather

92 than open-loop mode. Avoiding open-loop resonances places further constraints on model  
93 parameters.

94

95 We conclude that all constraints can be simultaneously satisfied, and that accommodation can  
96 be modelled successfully as a predictive system with integral control, but that there are fairly  
97 tight constraints on the gain and time-constant of the integral controller in order for the system  
98 to be consistent with empirical data for step and smooth tracking. Following previous work,  
99 we add a slow, second-order integral controller to account for adaptation effects, and show that  
100 care is required when using this dual-control with predictive models.

101

102 Our inclusion of noise leads us to propose adding one further component to the model  
103 developed so far: namely a non-predictive proportional-control signal, clipped at low values.  
104 We originally rejected non-predictive control because it is prone to closed-loop resonances at  
105 particular frequencies. This is because the phase of the cycle where demand is high causes an  
106 increase in accommodation designed to null the defocus error, but – due to the latency – by the  
107 time the increase in accommodation has taken effect, the demand cycle has moved on to a  
108 phase where demand is low, and so the increase in accommodation in fact enhances the defocus  
109 error, causing a larger change in accommodation in the next cycle, and so on. We can limit the  
110 destabilizing effect of this signal by making it saturate at low values. This ensures that it has  
111 little influence on accommodation in general, which remains dominated by the predictive  
112 integral control discussed above. However, the closed-loop resonance associated with non-  
113 predictive control remains detectable for small changes in demand. This amplifies noise within  
114 particular bandwidths, and means that the microfluctuations in the steady-state response show  
115 a peak at frequencies just over 1Hz, as observed. Opening the loop cuts the feedback pathway  
116 generating the resonance, explaining why this peak in the microfluctuation power spectrum is  
117 much less prominent in open-loop mode. The saturating proportional signal also accounts for  
118 the non-linear resonance observed when accommodation tracks low-amplitude – but not high-  
119 amplitude – sinusoidal oscillations in demand.

120

121 Putting these different components together results in a model where accommodation is  
122 controlled by the sum of four separate neural signals. The model has a total of ten parameters  
123 (Table 2), most of which are quite tightly constrained by the data. In Section 3, we present

124 simulation results demonstrating that this model can account simultaneously for a wide range  
125 of observations.

126

127

128

## 129 Methods

### 130 Accommodation as a linear, time-invariant negative feedback control system

131

132 “A complex system that works is invariably found to have evolved from a simple system that  
133 worked. A complex system designed from scratch never works and cannot be patched up to  
134 make it work. You have to start over with a working simple system.” – Gall’s Law (Gall, 1977).

135

136 In the spirit of Gall’s Law, we begin with the simplest possible conceptual model of  
137 accommodation (Figure 2). Viewed as a whole, the model has one input, *accommodative*  
138 *demand*, corresponding to the vergence of light rays from the object we wish to look at. This  
139 is measured in diopters; the demand in diopters corresponds to the reciprocal of the distance in  
140 metres from the eye. For an infinitely far object, the demand is 0D; for an object at 50cm, the  
141 demand is 2D.

142

143 The model also has one output, *ocular accommodation*. When the eye is correctly  
144 accommodated, the accommodation will be equal to the demand so that the image is in focus  
145 on the posterior receptor layer of the retina. *Defocus* is the difference between the  
146 accommodative demand and the ocular accommodation, all measured in diopters. It acts as an  
147 error signal to the model. As discussed in the Introduction, we assume that defocus is a single,  
148 signed value which is somehow computed by the visual system from the retinal image (e.g.  
149 using blur, higher-order aberrations, longitudinal chromatic aberration etc (Burge & Geisler,  
150 2011; Cholewiak et al., 2018; Fincham, 1951; Kruger et al., 1993; Seidemann & Schaeffel,  
151 2002; Wilson et al., 2002)) and represented as a neural error signal; how this is achieved is  
152 beyond the scope of this paper. In our sign convention, positive defocus error means that the  
153 eye is not accommodating enough, i.e. the eye is focusing on a point more distant than the  
154 object of interest, so the ocular image is focused behind the retina. Positive defocus error should  
155 therefore stimulate an increase of accommodation. The accommodative control system takes  
156 the defocus error as input and uses it to compute a neural control signal (Figure 2). This neural

157 signal is then fed into the ocular plant, meaning the ciliary muscle, lens and other components.  
158 Changes in the neural signal thus change the ocular accommodation, which in turn affects the  
159 defocus error (since defocus is demand minus accommodation). The accommodative control  
160 system is designed to adjust accommodation so as to minimise the defocus error signal (Toates,  
161 1972). Thus, this is a negative feedback system.

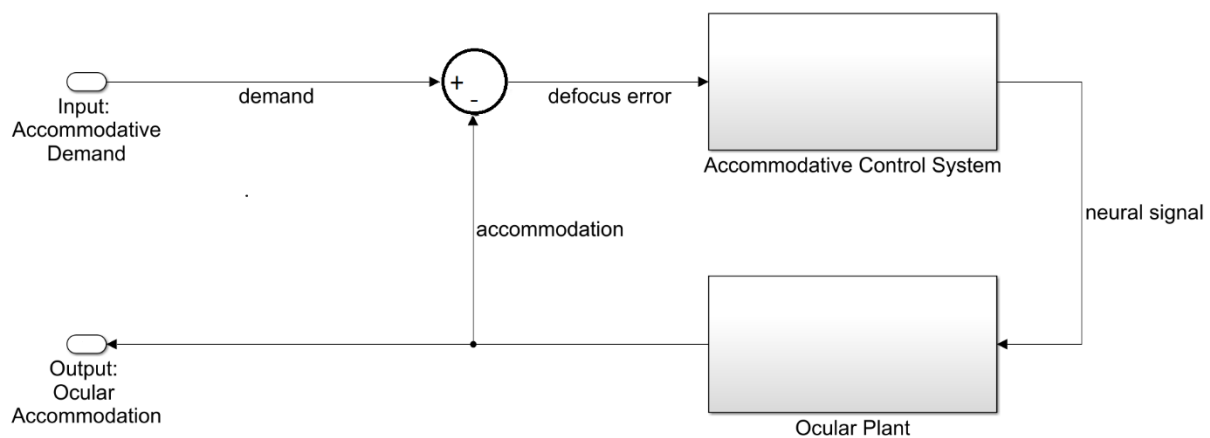
162

163 In any negative feedback system, one faces the question of how to choose the control signal so  
164 as to minimize the error. One obvious form of error correction is to make the corrective signal  
165 proportional to the error. For example, a very simple form of automotive cruise control might  
166 make acceleration proportional to the difference between the current and the desired speed.  
167 Other widely-used possibilities are to integrate the error over time, or to anticipate changes by  
168 including a term scaling with the derivative. Together, control systems of this type are called  
169 PID (proportional-integral-derivative) controllers.

170

171 In reality, of course, defocus is not the only cue to accommodation (Heath, 1956b; Maddox,  
172 1893). One additional component that we discuss below and include in our models is the  
173 system's bias towards a particular baseline or resting accommodation (see (Rosenfield et al.,  
174 1993a) for a review). Factors which for simplicity we neglect in this paper include pictorial  
175 cues to distance, sensed proximity and crosslinks from the vergence system. However, defocus  
176 is the only cue which is itself altered by accommodation, and thus the cue intrinsic to the  
177 negative feedback loop.

178



179

180

181 *Figure 2. Conceptual model of accommodation. All accommodative models in the literature fit into this basic schematic. There*  
182 *is a feedback loop, whereby the output (accommodation) affects the input to the control system. The blocks labelled*  
183 *Accommodative Control System and Ocular Plant are shown here as “black boxes” which take inputs and yield outputs,*  
184 *without showing how the output is computed. The input to the overall system is the accommodative demand, reflecting the*  
185 *distance of the fixated object, and the output is the ocular accommodation, i.e. where the eye is focused. Defocus error is the*  
186 *difference between these, demand minus accommodation.*

187

188

189 *Modelling neural signals as if they were in diopters*

190 In this initial part of the paper we will keep the discussion as general as possible, without  
191 committing to a particular model of the Ocular Plant or Accommodative Control System blocks  
192 shown in Figure 2. However, one detail is worth noting. Without loss of generality we will set  
193 the overall gain of the plant to 1, meaning that it passes a constant signal unchanged. In reality,  
194 the neural signal is encoded in spikes per second, and the output of the ocular plant is  
195 accommodation in diopters. There must therefore be a gain or conversion factor within the  
196 neural signal which converts spikes per second into diopters, taking into account the  
197 biomechanical gain of the plant (Gamlin et al., 1994) . Without loss of generality, we can fold  
198 this conversion factor into our neural signals. Thus by setting the plant gain to 1, we represent  
199 all the neural signals in the model as if they were diopters. This makes them particularly simple  
200 to interpret.

201

202 *Closed-loop versus open-loop*

203 The model shown in Figure 2 is “closed-loop”: that is, the input to the accommodative control  
204 system (defocus error) is affected by its output (ocular accommodation). As discussed, this  
205 forms a negative feedback loop, in which increases in defocus error stimulate changes in  
206 accommodation that in turn reduce defocus error.

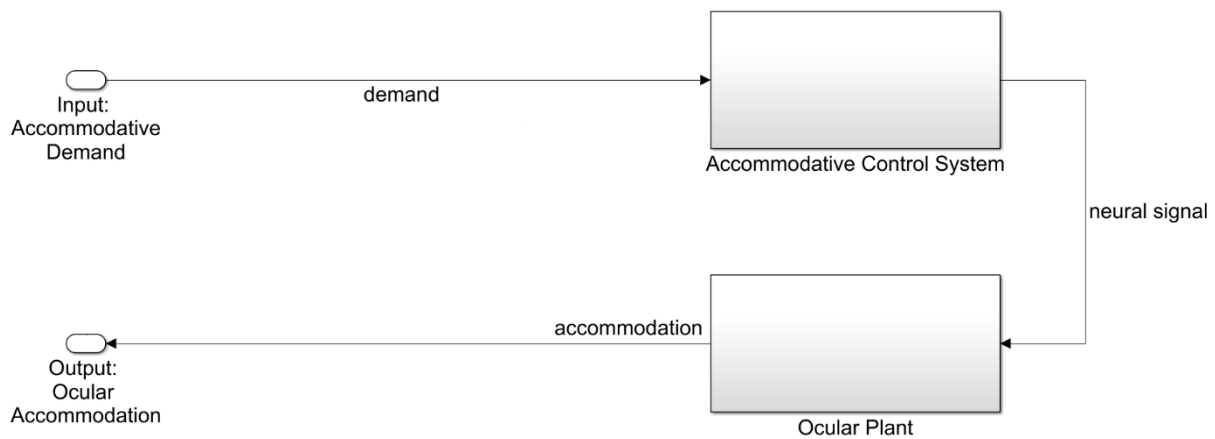
207

208 Figure 3 shows the equivalent open-loop system, in which the output of the system has no  
209 effect on its defocus error. It might seem impossible to “cut the wire” in this way in the living  
210 eye, but in fact all that is required to examine the open-loop mode is to make the optical error  
211 signal independent of the accommodative response. There are two main ways in which this can  
212 be done. First, by measuring accommodation and optically adding the current accommodation  
213 state onto the current input demand, as shown by the red text in Figure 4. The eye’s own optics  
214 then effectively removes accommodation, so that the error signal forming the input to the visual  
215 system is simply the demand applied by the experimenter, independent of the accommodative

216 response. A positive non-zero open-loop error signal continues to stimulate increases of the  
 217 accommodation response until it reaches saturation, reminiscent of a dog chasing its tail.

218  
 219 Alternatively, the optical error signal can be set to zero by using a pinhole pupil. Through small  
 220 pinholes, objects appear slightly blurred due to diffraction, but critically this blur is virtually  
 221 independent of the stimulus accommodative demand or the ocular accommodation. Pinholes  
 222 do not cause a “dog chasing tail” accommodative response, but rather accommodation tends to  
 223 assume its resting state. This suggests that the visual system experiences images seen through  
 224 pinholes as having zero defocus. Thus, viewing through pinholes is a special case of open-loop  
 225 in which the input is effectively clamped to zero regardless of output.

226

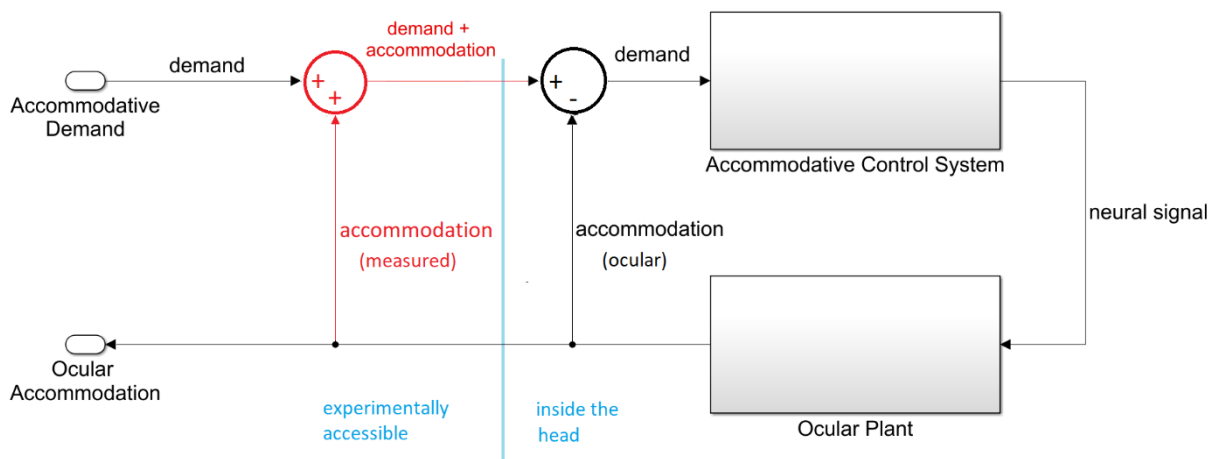


227

228 *Figure 3. An open-loop system: the inputs to the control system are independent of its outputs.*

229

230



231



232 *Figure 4. Accommodation driven in open-loop mode by adding the measured accommodation onto the input demand (red).*  
233 *The signal labelled “accommodation (ocular)” is the actual accommodation state of the eye, which is, as always, subtracted*  
234 *optically in the eye to yield defocus. The signal labelled “accommodation (measured)” is the value measured by the*  
235 *experimenter, which is artificially added onto the original demand signal at the red summation block. Ideally, the measured*  
236 *accommodation should be identical to the actual accommodation, and so the ocular accommodation is perfectly cancelled*  
237 *out by the addition of the measured accommodation. Thus, the error signal input to the block labelled Accommodative Control*  
238 *System remains equal to the applied demand, regardless of the accommodative response. This system is therefore equivalent*  
239 *to the simpler one shown in Figure 3 and is so operated in open-loop mode. Effectively, the red measured accommodation*  
240 *signal “cuts the loop” represented by the ocular accommodation. In this figure, the blue line separates signals which are*  
241 *outside the head and thus accessible for non-invasive experimental manipulation (the original demand and the measured*  
242 *accommodation signal which is added onto it) from signals which are in the eye/brain and thus not easily manipulable.*

243

244

245 *Primer on control system theory*

246 At this point, we note that vision scientists may not be familiar with the classical control  
247 systems approach taken in this paper. This section aims to provide a bare-bones introduction  
248 to enable such readers to follow subsequent sections. Table 1 provides a reference for all the  
249 symbols used throughout the paper.

250

251 *Linear time-invariant (LTI) systems and the Laplace domain*

252 Linear systems are those whose outputs for a linear combination of inputs are the same as a  
253 linear combination of individual responses to those inputs. For example, in Figure 2, if the  
254 system were linear, then if demand timecourse  $d_1(t)$  elicited accommodation response  $a_1(t)$ ,  
255 and demand  $d_2(t)$  elicited  $a_2(t)$ , the response to a new demand made up of a weighted sum of  
256 these two timecourses,  $w_1d_1(t)+w_2d_2(t)$  would be  $w_1a_1(t)+w_2a_2(t)$ . A time-invariant system is  
257 one where the same input, delayed by a time  $T$ , will always elicit the same response, also  
258 delayed by a time  $T$ . Thus if demand  $d_1(t)$  elicited accommodation response  $a_1(t)$ , demand  $d_1(t-$   
259  $T)$  would elicit accommodation response  $a_1(t-T)$ .

260

261 Where a system is both linear and time-invariant (LTI), its response can be analysed using  
262 Laplace transforms of the variables. The Laplace transform turns integral and differential  
263 equations into polynomial equations which are much easier to solve. Time-domain functions  
264 are converted into Laplace-domain functions of a complex frequency variable  $s$ . We assume  
265 that all signals are zero for times before  $t=0$ , and write the Laplace transform of a signal  $f(t)$  as  
266  $F(s)$ , where

267

268

$$F(s) = \int_0^{\infty} dt f(t)e^{-st}$$

269

Equation 1

270 We will adopt the convention where when a lower-case variable represents a function of time  
271  $t$ , the corresponding upper-case denotes its Laplace transform as a function of  $s$ . The Laplace  
272 transform is closely related to the Fourier transform with which vision scientists are typically  
273 more familiar, with  $s$  representing a complex version of angular temporal frequency:  $s=j\omega$   
274 (where we use  $j$  for the square root of -1 throughout).

275

276 In a circuit diagram like Figure 2, the effect of an LTI block is simply to reweight the amplitude,  
277 and/or shift the phase, of each frequency in the input. This means that each LTI block can be  
278 written simply in terms of its complex *transfer function*  $H(s)$ . As discussed in more detail  
279 below, a transfer function  $H(s)$  is a kind of gain, since it is the ratio of the output to the input,  
280 for each frequency  $s$ . For example, consider a transport delay block, whose effect is to delay  
281 the input signal by a latency  $T$ , and which thus shifts the phase of each frequency. If the input  
282 signal is  $i(t)$ , the output after delay is  $o(t) = i(t-T)$ . Substituting this into Equation 1, we find  
283 that

284

$$O(s) = \int_0^{\infty} dt o(t)e^{-st} = \int_0^{\infty} dt i(t-T)e^{-st} = \int_{-T}^{\infty} dt i(t)e^{-st-sT} = e^{-sT} I(s)$$

285

Equation 2

286 where we used the fact that  $i(t)=0$  for  $t<0$ . Thus, the transfer function of a transport delay block  
287 is  $H(s)=\exp(-sT)$ .

288

289 In LTI systems, one can do algebra on the Laplace transforms in the usual way. The transfer  
290 function for several LTI systems in parallel is the sum of the individual transfer functions,  
291 while the transfer function for several LTI systems in series is the product of the transfer  
292 functions for the individual systems.

293

294 *A mathematical trick to handle rest focus*

295 When viewing through pinholes, although the demand is zero, accommodation tends not to be  
296 zero but to converge on a “rest focus”,  $a_{RF}$ , generally of around 1.4D (Leibowitz & Owens,  
297 1978; Rosenfield et al., 1993b). A similar default focus is also observed in darkness. To account

298 for this, we assume that the accommodative control system adds onto the signal computed from  
299 defocus a constant “bias” signal. Because we have normalized neural signals to be expressed  
300 in diopters, setting this bias signal equal to the rest focus ensures that accommodation returns  
301 to the rest focus if the defocus error is clamped at zero.

302

303 This bias signal leads to a small complication, because it technically violates the assumption  
304 that all signals are zero for  $t < 0$ . To handle this, we express both accommodation and demand  
305 relative to the rest focus. We define  $A(s)$  to be the Laplace transform, not of accommodation  
306 itself, but of accommodation relative to rest focus,  $a(t) - a_{RF}$ . Similarly  $D(s)$  is the Laplace  
307 transform of demand relative to rest focus,  $d(t) - a_{RF}$ . With this trick, we can then analyse the  
308 system in the Laplace domain as if there were no bias signal ( $a_{RF} = 0$ ), and at the end simply add  
309  $a_{RF}$  back on to demand and accommodation when we move back to the time domain. All the  
310 analyses in this paper use this approach.

311

#### 312 *Open- and closed-loop transfer functions*

313 In Figure 3, where accommodation is driven in open-loop mode, we have

314

$$A(s) = P(s)B(s)D(s)$$

315 where  $B(s)$  is the transfer function representing the brain’s accommodative control system and  
316  $P(s)$  that representing the ocular plant. As described in the previous section,  $A(s)$  and  $D(s)$  are  
317 the Laplace transforms of accommodation and demand relative to rest focus. The open-loop  
318 transfer function relating output  $A(s)$  (accommodation) to input  $D(s)$  (demand) is thus

319

$$H_{open}(s) = \frac{A(s)}{D(s)} = P(s)B(s)$$

320

*Equation 3*

321

322

323 In the closed-loop mode shown in Figure 2, the input to the accommodative control system is  
324 defocus error,  $E(s) = D(s) - A(s)$ . We therefore now have

325

$$A(s) = H_{open}(s)[D(s) - A(s)]$$

326 and thus derive the closed-loop transfer function:

327

$$H_{closed}(s) = \frac{H_{open}(s)}{1 + H_{open}(s)}$$

328

*Equation 4*

329 where

$$330 \quad A(s) = H_{closed}(s)D(s)$$

331 This relationship between the open- and closed-loop transfer functions is a standard result for  
332 a feedback loop like the one in Figure 2.

333

### 334 *Steady-state response*

335 LTI theory shows that the steady-state response is obtained by evaluating the system at  $s=0$   
336 (zero frequency). So, if we apply a constant demand  $d_{ss}$  in closed-loop mode, we have

$$337 \quad A(0) = H_{closed}(0)D(0)$$

338

*Equation 5*

339 where  $D(0)=d_{ss}-a_{RF}$  and  $A(0)=a_{ss}-a_{RF}$  (recalling that accommodation and demand are defined  
340 relative to rest focus  $a_{RF}$ ). From Equation 4, we can write  $H_{closed}(0)$  in terms of  $H_{open}(0)$ . It  
341 will be convenient to introduce the notation  $G_{open}$  for  $H_{open}(0)$ , i.e. the open-loop steady-state  
342 gain of the system. Putting this together with Equation 4 and Equation 5, we find that  
343 accommodation will eventually be

$$344 \quad a_{ss} = a_{RF} + \frac{G_{open}}{1 + G_{open}} (d_{ss} - a_{RF})$$

345

*Equation 6*

346 The steady-state defocus error is

$$347 \quad d_{ss} - a_{ss} = \frac{d_{ss} - a_{RF}}{1 + G_{open}}$$

348

*Equation 7*

349 Equation 7 shows that – regardless of the control system or plant – the defocus error will be  
350 zero when the demand is equal to the rest focus. This is natural enough, since the rest focus is  
351 the value to which the system is biased.

352

353 However, for other demands, the steady-state error is not zero. When the demand is nearer than  
354 the rest focus, the accommodative response remains further than the demand, a situation  
355 referred to as accommodative lag. Conversely when demand is further than rest,  
356 accommodation is nearer than demand; this is accommodative lead.

357

358 Importantly, the amount of the error depends on the steady-state open-loop gain  $G_{open}$ . This  
359 demonstrates an important property of negative-feedback systems which attempt to minimise

360 error: small error requires high open-loop gain. Since we have set the gain of the plant to 1  
361 (without loss of generality, as noted above), the gain  $G_{open}$  is set entirely by the brain's  
362 accommodative control system. Empirically, accommodation reaches around 80%-90% of the  
363 demand when the demand is far from the rest focus. From Equation 4, we have

$$364 \quad \frac{a_{ss} - a_{RF}}{d_{ss} - a_{RF}} = \frac{G_{open}}{1 + G_{open}}$$

365 so the observation that accommodation is around 80-90% of demand implies that  
366  $G_{open}/(1+G_{open})$  is around 0.8-0.9, and in turn that  $G_{open}$  must be in the range 4-9.

367

### 368 *Gain and phase of response to sinusoidal inputs*

369 A property of any LTI system is that (after initial onset transients have died away) its response  
370 to a sinusoidal input is a sinusoidal output, with a gain and phase reflecting the transfer function  
371 of the system. Specifically, if the closed-loop transfer function is  $H_{closed}(s)$ , then if  
372 accommodative demand is a sinusoidal function of time, the accommodative response will also  
373 be a sinusoid with the same temporal frequency  $f$ . The amplitude of the response will be the  
374 amplitude of the demand multiplied by the gain at that frequency,  $g(f)$ , and the phase will be  
375 delayed by  $\phi(f)$ . We will use lower-case  $g(f)$  to denote the gain of a system at a particular  
376 temporal frequency  $f$ , and upper-case  $G=g(0)$  to denote the steady-state gain, as we did above  
377 for  $G_{open}$ . According to a standard result of LTI theory, the gain and phase-delay of an LTI  
378 system at frequency  $f$  can be obtained from the complex number represented by its transfer  
379 function  $H(s)$  evaluated at  $s=2\pi jf$ . The gain  $g(f)$  is the magnitude of the complex number  
380  $H(2\pi jf)$  and the phase-delay  $\phi(f)$  is its phase.

381

382 Sometimes below for brevity we will refer to “the gain” of an LTI operator, without specifying  
383 a frequency. In this case, we mean its steady-state gain. For example, when we refer to “the  
384 gain” of a low-pass filter, we mean the ratio of its steady-state output to a constant input.

385

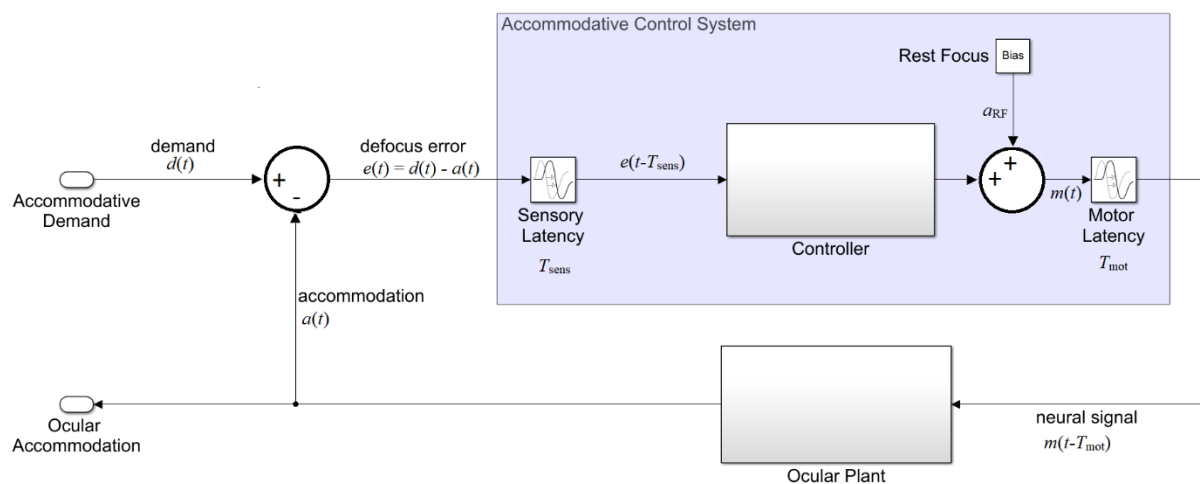
### 386 *Sensorimotor latencies: a problem for control*

387 These preliminaries out of the way, we now consider different possibilities for the contents of  
388 the block labelled Accommodative Control System in Figure 2. We begin by expanding this  
389 block as shown in Figure 5. We now explicitly include the rest focus signal discussed above.  
390 But critically, Figure 5 now also shows the system's latency, which we have divided into two  
391 parts. The first is an afferent-sensory latency, representing the time taken for information about  
392 the retinal image to travel up the optic nerve and for the brain to compute a signed estimate of

393 defocus, for example using longitudinal chromatic aberration or higher-order aberrations. The  
 394 second is an efferent-motor latency, representing the time taken for the resultant neural signal  
 395 to travel from the Edinger-Westphal nucleus down the IIIrd cranial nerve and reach the ciliary  
 396 muscle. These have been estimated as  $T_{sens} \sim 200\text{ms}$  and  $T_{mot} \sim 100\text{ms}$  respectively (Gamlin et  
 397 al., 1994; Schor et al., 1999; D. Wilson, 1973). In Figure 5, these latencies are shown within  
 398 the Accommodative Control System, i.e. the brain, but the model functioning is unchanged if,  
 399 for example, part of the motor latency occurs at a neuromuscular junction in the eye, or indeed  
 400 if both latencies are merged into a single block.

401

402



403

404 *Figure 5. Expanding the conceptual model shown in Figure 2 so as to show the rest focus and sensorimotor latencies. This is*  
 405 *the same circuit diagram, but the block labelled Accommodative Control System has here been expanded to explicitly show*  
 406 *the constant bias signal accounting for the rest focus, and the latencies. There is a sensory latency  $T_{sens}$  before the retinal*  
 407 *defocus signal reaches the controller, and a further motor latency  $T_{mot}$  before the neural signal reaches the plant.*

408

409 Latencies are a potentially serious problem for any control system. In the block diagram shown  
 410 in Figure 5, we can see that the defocus error only becomes available to the block marked  
 411 Controller after the sensory latency. The controller therefore operates not on  $e(t)$ , but  $e(t - T_{sens})$ :  
 412 the retinal defocus as it was a time  $T_{sens}$  ago. This in turn reflects the accommodation due to the  
 413 neural signal sent up to a time  $T_{sens} + T_{mot}$  ago. Thus, the system suffers an overall latency of  $T_{lat}$   
 414  $= T_{sens} + T_{mot}$ . This can easily lead to overshoots and “ringing”: oscillations in accommodation  
 415 as the system is driven beyond the correct value by the out-of-date error signal.

416

417 Overshoots and ringing due to an out-of-date error signal would be seen with the response to  
418 step changes in demand, but in fact the second-order dynamics already indicate that LTI models  
419 do not suffice to account for the response to large step changes; accommodative control seems  
420 to have special mechanisms for these which are beyond the scope of this paper (Bharadwaj &  
421 Schor, 2005, 2006; Schor & Bharadwaj, 2005, 2004). However, an out-of-date error signal  
422 would also affect the response to sinusoidal oscillations in demand which we are concentrating  
423 on here.

424

425 Empirically, accommodation shows a low-pass response: gain is greatest in the steady-state,  
426 and decreases monotonically with temporal frequency (Charman & Heron, 2000; Krishnan et  
427 al., 1973; Kruger & Pola, 1986; Ohtsuka & Sawa, 1997; Stark et al., 1965). However, it is  
428 challenging to achieve this with the circuit diagram shown in Figure 5 and a Controller block  
429 which is simply a PID controller. Because of the latency, the system can easily end up out of  
430 phase, so that the changes in accommodation actually enhance the defocus rather than reducing  
431 it, as intended. This shows up as resonances or local peaks in the gain function, making it non-  
432 monotonic. This is not observed empirically. To avoid this, the controller must be more  
433 complex, as shown in Figure 6.

434

435 [Overcoming latencies with a predictive control system: the Smith Predictor](#)

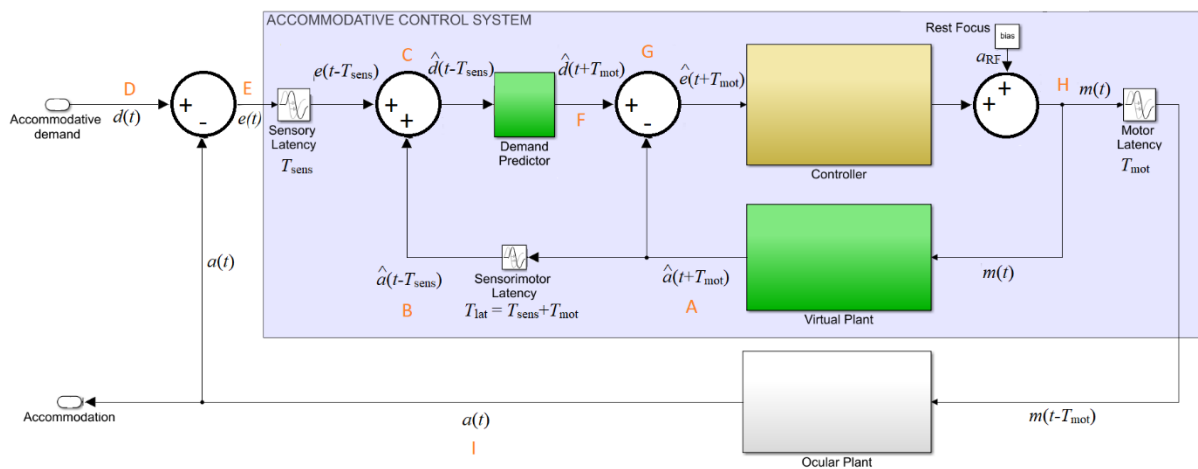
436 The solution seems to be that the visual system actually bases its neural control not on the  
437 currently available sensed value of retinal defocus, but on its internal prediction of the *future*  
438 retinal defocus. That is, whereas in Figure 5 the controller operates on the sensed defocus,  
439 which due to the sensory latency actually represents defocus as it was some time in the past, in  
440 a predictive model the controller operates on the *predicted future* defocus (Smith, 1957).  
441 Figure 6 shows how Figure 5 can be modified so that the input to the controller is predicted  
442 future defocus. Defocus is the difference between the stimulus accommodative demand and the  
443 ocular accommodation, so predicting future defocus requires a prediction both of demand and  
444 accommodation.

445

446 The brain is in principle able to predict accommodation perfectly up to future times less than  
447 the motor latency, simply based on the signals it has already sent to the accommodative plant.  
448 (Campbell & Westheimer, 1960; Hung et al., 2002; Krishnan et al., 1973; Schor & Bharadwaj,  
449 2004; Stark et al., 1965; F. Sun et al., 1989) To do this, the visual system must effectively have  
450 its own internal model of the ocular plant, represented by the *Virtual Plant* block in Figure 6.

451 Such internal models are referred to as *forward models* in control systems theory. We assume  
 452 that the motor latency  $T_{\text{mot}}$  largely represents delays in transmitting the control signal from the  
 453 brain to the eye. We assume that the virtual plant is located in the brain close to where the  
 454 neural control signal is generated, and thus has access to this signal with negligible delay.  
 455 Accordingly, the output of the virtual plant is *predicted future accommodation*, i.e. the value  
 456 that ocular accommodation will have at a time  $T_{\text{mot}}$  in advance of the present. We write this  
 457 predicted future accommodation as  $\hat{a}(t+T_{\text{mot}})$ : the predicted accommodation at a time  $T_{\text{mot}}$  in  
 458 the future, where the circumflex indicates that this is an *estimate* of the future accommodation.  
 459 Since the accommodation up to a time  $T_{\text{mot}}$  into the future is controlled by neural signals already  
 460 sent by the brain, this estimate can in principle be perfect. It should be affected only by noise,  
 461 and by any inaccuracies in the virtual plant as a model of the ocular plant. In the model we  
 462 present here, neither of these apply and so the prediction of future accommodation is indeed  
 463 perfect.

464  
 465



466  
 467 *Figure 6. Predictive control. Compare with Figure 5: the Controller block has been replaced with a more complex system*  
 468 *including two predictive blocks (green) as well as the original Controller block (yellow). The prediction helps avoid instability*  
 469 *due to the sensorimotor latencies. To predict accommodation, the model includes a Virtual Plant block (forward model) to*  
 470 *compute what accommodation will be a time  $T_{\text{mot}}$  in the future, i.e. after the motor latency. If the forward model is accurate,*  
 471 *this can in principle predict accommodation perfectly up to  $t+T_{\text{mot}}$ , since accommodation is under the system's own control.*  
 472 *To predict demand at time  $T_{\text{mot}}$  into the future, the model uses a Demand Predictor block. This requires extrapolating demand*  
 473 *at time  $T_{\text{lat}}=T_{\text{sens}}+T_{\text{mot}}$  beyond the last available estimate. This is unlikely to be entirely accurate, since demand can reflect*  
 474 *changes in the outside world, beyond the system's control. Orange labels indicate locations referred to in the text.*

475



476 Predicting stimulus demand is more challenging, since in general this reflects the motion of  
477 objects in the outside world. Nevertheless, several studies (Campbell & Westheimer, 1960;  
478 Charman & Heron, 2000; Krishnan et al., 1973; Phillips et al., 1972; Stark et al., 1965) have  
479 suggested that the accommodation system, like other motor systems, may be capable of  
480 predicting sufficiently regular input. For example, if the demand is a square wave, jumping  
481 between two values with a constant period, accommodation develops a very short latency or  
482 even changes in anticipation (Krishnan et al., 1973). How or whether this prediction is achieved  
483 is beyond the scope of this paper; it may be performed by the cerebellum (Ohtsuka & Sawa,  
484 1997; Popa & Ebner, 2019) or it may not actually occur (Águila-Carrasco & Marín-Franch,  
485 2021; Otero et al., 2019). The different possibilities can be modelled with the *Demand*  
486 *Predictor* block (Figure 6). As will become clear below, the Demand Predictor block takes as  
487 its input what demand is estimated to have been at time  $T_{sens}$  in the past,  $\hat{d}(t - T_{sens})$ , and gives  
488 as output what it estimates demand will be at time  $T_{mot}$  in the future,  $\hat{d}(t + T_{mot})$ . That is, it  
489 needs to extrapolate its input into the future by a time corresponding to the entire sensorimotor  
490 latency,  $T_{lat} = T_{mot} + T_{sens}$ . In this paper, our model Demand Predictor block will simply pass its  
491 input on unchanged, effectively assuming that the demand will stay at its current value. A future  
492 model could incorporate a more elaborate form of prediction, e.g. taking account of stimulus  
493 periodicity, but that is beyond the scope of this paper.

494  
495 Having introduced the key elements of the predictive model – the virtual plant and the demand  
496 predictor – we now discuss how it works. To help with this, we have annotated the signals in  
497 Figure 6 and marked some reference points with orange letters. Let's start at A with the output  
498 of the virtual plant. As we saw above, this represents the brain's prediction of what ocular  
499 accommodation will be at time  $T_{mot}$  in the future:  $\hat{a}(t + T_{mot})$ . Our model brain uses this  
500 predicted future accommodation in two ways. First (B), the model brain delays this predicted-  
501 accommodation signal by the total sensorimotor latency to obtain  $\hat{a}(t - T_{sens})$ , an estimate of what  
502 the ocular accommodation was at a time  $T_{sens}$  in the past. Thus, the predictive model actually  
503 uses an internal estimate of *past* accommodation as well as of future accommodation. The point  
504 of doing this is to match the latency of the defocus signal. The input to the whole system is  
505 accommodative demand,  $d(t)$  (label D). In the eye (label E), the ocular accommodation  $a(t)$  is  
506 optically subtracted from  $d(t)$  to yield the error signal  $e(t)$ , the defocus at time  $t$ . Ideally, this is  
507 what the accommodation control should be based on, but due to the sensory latency  $T_{sens}$ , the  
508 brain only has access to the delayed signal,  $e(t - T_{sens})$ , representing the defocus at a time  $T_{sens}$

509 ago. At the signal combination labelled C, the brain adds its estimate of past accommodation,  
510  $\hat{a}(t-T_{\text{sens}})$ , back onto this delayed defocus signal  $e(t-T_{\text{sens}})$ , in order to obtain an estimate of what  
511 the demand was at a time  $T_{\text{sens}}$  in the past:  $\hat{d}(t - T_{\text{sens}}) = e(t - T_{\text{sens}}) + \hat{a}(t - T_{\text{sens}})$ . This  
512 demand signal is fed into the Demand Predictor block, which uses it to make a guess at what  
513 the demand will be at a time  $T_{\text{mot}}$  in the future:  $\hat{d}(t + T_{\text{mot}})$  (label F).

514

515 Now, the brain makes its second use of predicted future ocular accommodation, this time  
516 without applying any delay. At the signal combination labelled G, it subtracts the predicted  
517 accommodation  $\hat{a}(t + T_{\text{mot}})$  from the predicted demand  $\hat{d}(t + T_{\text{mot}})$  to obtain the predicted  
518 future defocus:  $\hat{e}(t + T_{\text{mot}}) = \hat{d}(t + T_{\text{mot}}) - \hat{a}(t + T_{\text{mot}})$ . This predicted future defocus is  
519 what is fed into the yellow Controller block and used to compute the neural control signal  
520 driving accommodation. It is this use of predicted future defocus which makes this a predictive  
521 model, as compared to the model shown in Figure 5.

522

523 As noted above, a constant bias is added on to the output of the controller, which accounts for  
524 the non-zero resting focus. We call the result  $m(t)$  (label H). This is the actual motor signal sent  
525 to the ocular plant, with a latency  $T_{\text{mot}}$ , which results in the ocular accommodation  $a(t)$  (label  
526 I). An efference copy of the same motor signal is also sent to be the input of the virtual plant.  
527 The output of the virtual plant is, of course, the predicted future accommodation that we began  
528 with (A), so we have now followed the signals around the whole of the inner loop.

529

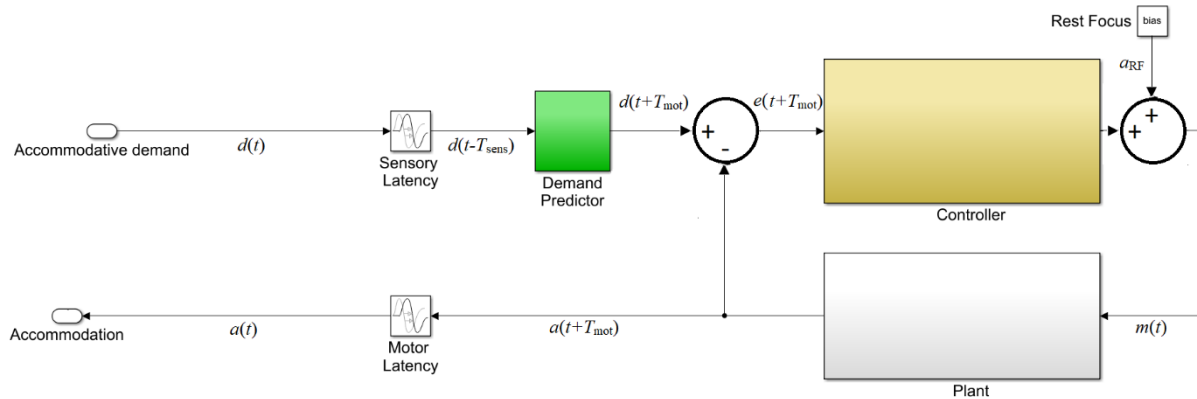
530 In summary, then, although the input to the accommodative control system as a whole is the  
531 *current* optical defocus (Figure 2), in a predictive model the input to the accommodative  
532 controller itself is the predicted *future* defocus. With this modification, PID-type controllers  
533 can now work well and avoid the instabilities associated with an out-of-date error signal.

534

535 [Simplified representation of the predictive control system](#)

536 If the virtual plant is a perfect simulation of the physical plant, the predictive control system  
537 shown in Figure 6 is mathematically equivalent to the much simpler form shown in Figure 7.  
538 This form can appear confusing, because it shows accommodation being subtracted from the  
539 stimulus demand *after* the sensory latency (even though some of the sensory delay represents  
540 the optic nerve and cortical processing) and *before* the motor latency (even though that  
541 represents processes before accommodation). It is important to remember that apparently “non-

542 causal” model diagrams like Figure 7 are a shorthand representing physiological predictive  
 543 models like Figure 6, for the case where the virtual plant model is perfect. The reader is invited  
 544 to trace the signals around Figure 6 and Figure 7, and verify that provided  $\hat{a}(t)=a(t)$ , the same  
 545 inputs are fed into the same blocks and so the results must be the same. This can facilitate  
 546 mathematical analysis.  
 547



548  
 549 *Figure 7. Simplified version of the model shown in Figure 6. This “non-causal” model structure is not physiological and cannot*  
 550 *be mapped onto “brain” and “eye” like the predictive physiological model in Figure 6. For example, here the single block*  
 551 *labelled “Plant” is used to represent both the physical plant in the eye and the virtual plant modelled in the brain. However,*  
 552 *as shown by the annotated signals, it is mathematically equivalent to the physiological model in Figure 6, provided that the*  
 553 *Virtual Plant block is a perfect simulation of the Ocular Plant.*

554  
 555 Transfer function of the predictive control system  
 556 The transfer function of this predictive model depends on the form of the demand predictor.  
 557 We can distinguish two extreme cases: perfect vs “no change” prediction.

558 *(i) Perfect prediction*

559 It is helpful to consider the unattainable ideal case in which the *Demand Predictor* block  
 560 perfectly predicts the demand at a time  $T_{sens}+T_{mot}$  beyond the last available information:

561 
$$\hat{d}(t + T_{mot}) = d(t + T_{mot})$$

562 In this case, the closed-loop transfer function is

563 
$$H_{closed}^{perfect}(s) = \frac{P(s)C(s)}{P(s)C(s) + 1}$$

564 *Equation 8*

565 With perfect prediction, the sensorimotor latency has no effect at all on the gain or phase or  
 566 indeed any other aspect of the response, since the perfect prediction annuls its effect.

567

568 (ii) “No change” prediction

569 In many natural viewing situations, accommodative demand probably often changes rather  
570 little over the timescale of  $T_{lat}$ . Thus it may be relatively safe to adopt an attitude of “*plus ça*  
571 *change, plus c’est la même chose*” and assume that the demand at future time  $t+T_{mot}$  will be the  
572 same as it was at the past time  $t-T_{sens}$ . In this case, the demand predictor block simply passes  
573 through its input as output:

$$574 \hat{d}(t + T_{mot}) = d(t - T_{sens})$$

575 Equation 9

576 In this case, the overall closed-loop transfer function is

$$577 H_{closed}^{nochange}(s) = \frac{P(s)C(s) \exp(-sT_{lat})}{1 + P(s)C(s)}$$

578 Equation 10

580 This is the simplest possible form of prediction: assuming things will stay the same as they are  
581 right now. And yet interestingly, the gain is exactly the same as for perfect prediction.  
582 Mathematically, this is because latency appears only in the numerator of Equation 10, and thus  
583 does not affect the magnitude of the complex transfer function,  $|H_{closed}^{nochange}(j\omega)|$ , which is what  
584 controls the gain at a given frequency (see Table 3). This means that the prediction of  
585 accommodation performed by the virtual plant suffices to avoid instability due to the latency,  
586 even if the “prediction” of demand is simply to assume it remains constant. Similarly, we can  
587 see that the phase of the “no change” transfer function is equal to the phase of the “perfect  
588 prediction” transfer function, plus a term  $\omega T_{lat}$  reflecting the sensorimotor latency. In other  
589 words, the response of the “no change” predictive model to sinusoids is exactly the same as  
590 the perfect predictive model, but delayed by the sensorimotor latency. This suggests that  
591 whereas predicting accommodation confers stability, the advantage of predicting demand is  
592 not stability, but shorter phase-delay and thus a more rapid response.

593

594

595 [A specific model of accommodative control](#)

596 So far we have deliberately kept the discussion very general, without committing to a particular  
597 choice of transfer function for either the ocular plant or the Controller block which converts  
598 defocus into a neural signal to the plant. In this section, we develop and justify a more specific

599 model of accommodative control. We discuss plausible assumptions and constraints on both  
600 the forms of these transfer functions, and their particular parameters.

601 *Ocular plant*

602 The ocular plant can be regarded at least roughly as a first-order leaky integrator or low-pass  
603 temporal filter (A. P. A. Beers & Van Der Heijde, 1994; A. P. Beers & van der Heijde, 1996;  
604 Ejiri et al., 1969). We therefore model the transfer function of the plant as

$$605 \quad P(s) = \frac{1}{1 + \tau_{plant}s}$$

606 *Equation 11*

607 where empirically  $\tau_{plant}$  is around 0.156s for young eyes (Schor & Bharadwaj, 2006). As noted  
608 above, we can assume without loss of generality that the steady-state gain of the plant is 1.

609 *Controller*

610 We now come to a key decision: the choice of transfer function for the Controller,  $C(s)$ . As  
611 noted above, in industrial control systems, controllers typically have proportional, integral and  
612 derivative (PID) terms, with transfer functions which scale as constant, 1/s or s respectively.

613 We can rule out pure proportional control, since with  $P(s)$  as given in Equation 11, making  
614  $C(s)$  constant means that the system tracks rapid sinusoidal oscillations far better than human  
615 accommodation. For example,  $C(s)=5$  results in a realistic steady-state gain of 83% (Equation  
616 6), but the gain remains >50% out to frequencies as high as 8Hz, far higher than observed (see  
617 Figure 8 below). Derivative terms do not affect steady-state error, but improve stability and  
618 avoid overshoot. They also enable rapid response to rapid changes. However, they can be  
619 problematic in the presence of noise. Previous work by Schor and Bharadwaj (Bharadwaj &  
620 Schor, 2006; Schor & Bharadwaj, 2006, 2004) suggests that the accommodative system has a  
621 distinct “pulse” mechanism for responding to sudden large changes in accommodation such as  
622 occur when we change from looking at a distant to a near object, which cannot be modelled by  
623 an LTI system and which are beyond the scope of this paper. Furthermore, many of the benefits  
624 of derivative control are already achieved by our use of a forward model to predict future  
625 demand. We therefore do not include a derivative term. This leaves us with the integral term.  
626 A pure integral controller has a transfer function proportional to 1/s, and thus infinite gain at  
627  $s=0$ . This is desirable since it eliminates steady-state error, but as noted, the human  
628 accommodation does not seem to completely eliminate steady-state error. We can account for  
629 this by modelling the controller as a leaky integrator, following Krishnan and Stark (Krishnan  
630 & Stark, 1975):

631 
$$C(s) = \frac{G_{fast}}{1 + s\tau_{fast}}$$

632 *Equation 12*

633 where  $G_{fast}$  is the steady-state gain and  $\tau_{fast}$  the time-constant. The subscript “fast” is to  
634 distinguish this from a slow integrator which we shall introduce below. A leaky integrator acts  
635 like a pure integral controller over short timescales ( $s\tau \gg 1$ ), and like a pure proportional  
636 controller over long timescales ( $s\tau \ll 1$ ), thus combining aspects of both. We noted above that  
637 accommodative lead/lag suggests the steady-state gain must be in the range 4-9. We somewhat  
638 arbitrarily chose  $G_{fast}=8$ .

639

640 Gain for sinusoidal input: sub-critical damping

641 With both the plant and the controller being leaky integrators, and with a predictive control  
642 system, the closed-loop gain is that of a damped harmonic oscillator (Equation 21, Appendix).  
643 The behaviour of this system can be summarised by its natural frequency and damping  
644 coefficient  $\zeta$ , both of which depend on the parameters  $G_{fast}, \tau_{fast}, \tau_{plant}$  (Equation 22). If the  
645 damping coefficient  $\zeta$  is too low, the maximum gain is observed for a non-zero resonance  
646 frequency, and can even exceed 1. This does not agree with empirical observations of  
647 accommodative response to sinewaves, which is low-pass (Charman & Heron, 2000; Kruger  
648 & Pola, 1986; Ohtsuka & Sawa, 1997; Stark et al., 1965); Figure 8A. This indicates that  $\zeta$  is at  
649 least  $1/\sqrt{2}$ , not far below critical damping ( $\zeta=1$ ) (Labhishetty & Bobier, 2017). Saccades have  
650 a damping coefficient of around 0.7 (Bahill et al., 1975); systems with this value have minimum  
651 settling time, i.e. they reach and remain within 5% of their final value most rapidly. We show  
652 in the Appendix that obtaining  $\zeta \sim 1/\sqrt{2}$  for a system with  $G_{fast} \gg 1$  requires the time-constant of  
653 the fast controller to be

654

655 
$$\tau_{fast} = 2G_{fast}\tau_{plant}$$

656 *Equation 13*

657 Thus, with  $\tau_{plant}=0.156s$  and  $G_{fast}=8$ ,  $\tau_{fast}$  must be at least 2.5s.

658

659 Phase for sinusoidal input: further evidence for predictive control

660 Empirically, up to  $\sim 1Hz$  the phase delay of accommodation is very close to a linear function  
661 of frequency, indicating a constant latency  $T_{delay}$  :  $\phi = 2\pi f T_{delay}$  (Charman & Heron, 2000;

662 Heron et al., 1999; Kruger & Pola, 1986; Ohtsuka & Sawa, 1997; Wildt et al., 1974). The slope  
663 usually corresponds to a delay of  $\sim 0.5$ s (dashed lines in Figure 8BC), though there is  
664 considerable variability between studies. Because this is close to the sensorimotor latency  
665 inferred from the response to step changes, it is often therefore assumed that this phase slope  
666 must represent the sensorimotor latency. However, this is not necessarily the case. First, the  
667 damped second-order system formed by the ocular plant and the neural control imposes delays  
668 in addition to the sensorimotor latencies. Second, in Equation 8 we saw that if the brain predicts  
669 demand perfectly – at least theoretically possible for a regular stimulus like a sinewave – then  
670 its phase delay becomes independent of the sensorimotor latency.

671

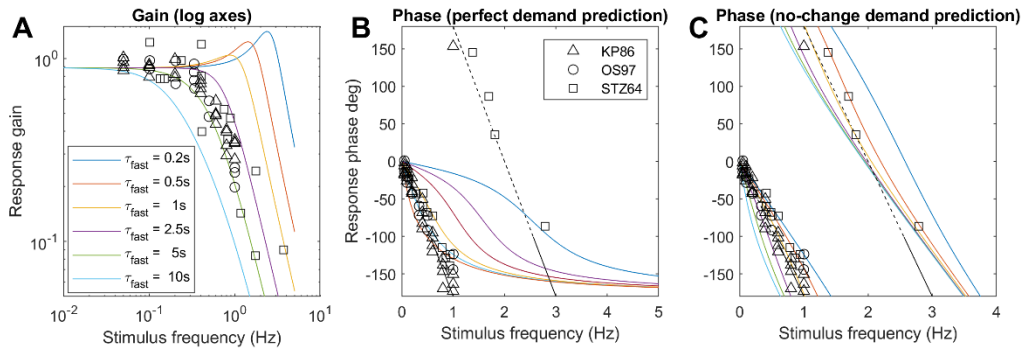
672 The time-constant of the fast integrator

673 Thus, together the gain and phase response of accommodation to sinusoidal oscillations in  
674 demand place quite tight constraints on the time-constant of the fast integrator,  $\tau_{\text{fast}}$ , given that  
675 the time-constant of the plant is a biomechanical given, and the gain of the fast integrator is  
676 already quite tightly constrained by the observed lead/lag following a change in demand.

677 Figure 8 illustrates this by comparing the theoretical gain and phase with different values of  
678  $\tau_{\text{fast}}$  with empirical results from various subjects and studies. As noted, we can rule out  $\tau_{\text{fast}} <$   
679  $2.5$ s because the gain is then too high at high frequencies. The gain data is probably best  
680 described by  $\tau_{\text{fast}} = 4$ s (green lines), but this does not account for the phase data.  $\tau_{\text{fast}} = 4$ s in the  
681 perfect-prediction model gives phases which match empirical data up to around  $0.5$ Hz, but at  
682 higher frequencies, empirical phase continues to increase roughly linearly, implying a constant  
683 delay, whereas phase for the perfect prediction model asymptotes at  $180^\circ$ . Thus, we probably  
684 have to reject the perfect-prediction model (not surprising given its idealised nature). The no-  
685 change prediction model is qualitatively in much better agreement with the phase data, but then  
686  $\tau_{\text{fast}} = 4$ s predicts larger phases than are observed. The purple line shows the curve with  
687 minimum settling time,  $\tau_{\text{fast}} = 2.5$ s which yields  $\zeta \sim 1/\sqrt{2}$ . This is in reasonable agreement with  
688 both gain and phase data, assuming simple no-change demand prediction, and we therefore  
689 adopt this value in the rest of the paper.

690

691



692

693 *Figure 8. Constraints on the time-constant of the fast integrator. Coloured lines show the gain and phase predicted for a*  
 694 *predictive model with leaky-integral control, Table 3, with  $P(s)$  given by Equation 11 with  $\tau_{plant}=0.156s$ , and  $C(s)$  given by*  
 695 *Equation 12 with  $G_{fast}=8$  and different choices of  $\tau_{fast}$ . The phase is shown for a model capable of predicting demand perfectly*  
 696 *(B), or for the “no-change” model which simply assumes demand will continue at its instantaneous value. Symbols show*  
 697 *empirical results from Kruger and Pola (1986), Ohtsuka and Sawa (1997), and Stark et al (1965). Code to generate this figure*  
 698 *is in Fig\_TimeConstraints.m. The dashed line in the phase plots corresponds to a constant latency of 0.5s, close to what is*  
 699 *observed.*

700

#### 701 Adaptation and dual control

702 Another distinctive feature of accommodation is that it adapts the open-loop decay time course  
 703 to resting position after prolonged exposure to the same demand. This can be revealed by using  
 704 pinholes to place the system in open-loop mode. As we have seen, in this situation,  
 705 accommodation relaxes back to the resting focus. After short periods of stimulation, this  
 706 happens rapidly, in a few seconds. However, after long periods of exposure to a particular  
 707 demand, the relaxation happens over a much longer time period, sometimes several minutes.  
 708 This cannot be accounted for with the leaky-integral control proposed so far. However, it can  
 709 be explained by positing a dual control system in which a fast, or phasic, neural integrator  
 710 controls changes in response amplitude and a slow, or tonic, neural integrator maintains the  
 711 response amplitude (Khosroyani & Hung, 2002; Schor, 1979a; Schor et al., 1986; F. C. Sun &  
 712 Stark, 1990).

713

714 The fast integrator is the one we have considered so far, which responds to error signals  
 715 computed from negative feedback. The slow integrator responds to the activity of the fast  
 716 neural integrator, and not directly to the error signal. As the name implies, the slow integrator  
 717 has a long time constant, which means that it has little effect on the response to rapid changes  
 718 in demand, so our previous discussion is not invalidated by its addition. With this arrangement,  
 719 the transfer function of the Controller becomes



720

$$C(s) = \frac{G_{fast}}{s\tau_{fast} + 1} \left( 1 + \frac{G_{slow}}{s\tau_{slow} + 1} \right)$$

722

*Equation 14*

723

724

725 The steady-state open-loop gain of the system is therefore

$$G_{open} = G_{fast}(1 + G_{slow})$$

727

*Equation 15*

728 Figure 9 shows the control system of Figure 5, modified to include this second, slow integrator,

729 since it is easier to appreciate its operation in a non-predictive system. Suppose the system

730 starts from rest, with demand and accommodation both equal to the rest focus, so that the

731 defocus error and the outputs of the fast and slow integrators are both zero and the neural signal

732 sent to the plant is simply the bias signal, maintaining it at the rest focus. Suppose the demand

733 then makes a step change to a nearer value,  $d_0$ . This in turn makes the defocus error non-zero,

734 which begins to charge up the fast integrator. This increases the neural signal  $m(t)$  above the

735 bias value, altering accommodation so as to reduce the error. It also begins to charge up the

736 slow integrator. Thus, over short timescales, the neural signal controlling accommodation is

737 set mainly by the output of the fast integrator. However, over long timescales, the slow

738 integrator takes over. The ratio of their steady-state contributions is equal to the gain of the

739 slow integrator (Schor, 1979b; Schor et al., 1986); for example, with our value  $G_{slow}=5$ , steady-

740 state accommodation is 83% due to the slow integrator and 17% due to the fast integrator.

741 Now suppose that pinholes are applied, making the defocus error zero regardless of

742 accommodation. In this non-predictive model, after a delay corresponding to the sensory

743 latency, the signal entering the fast integrator instantaneously drops to zero, and the fast

744 integrator begins to discharge. As the fast integrator discharges, accommodation drops rapidly,

745 with a decay time corresponding to  $\tau_{fast}$ . When the signal from the fast integrator has dropped

746 far enough, the slow integrator begins to discharge as well, resulting in a second, slower decay

747 of accommodation, with a time constant corresponding to  $\tau_{slow}$ . Thus, after a long period of

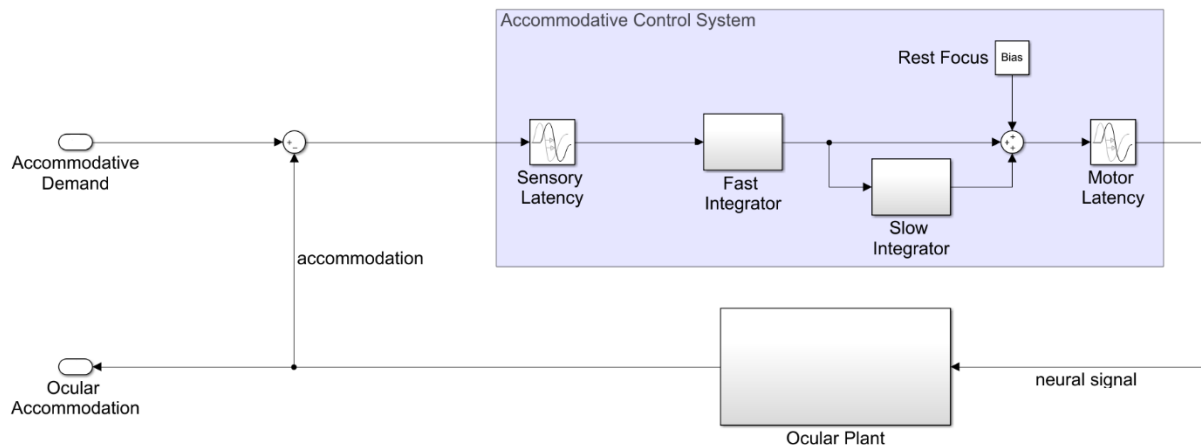
748 exposure, there is an initial rapid drop as the proportion of accommodation due to the fast

749 integrator, initially  $1/(G_{slow}+1)$ , decays rapidly, but then a much longer decay as the dominant

750 component due to the slow integrator decays slowly.

751

752



753

754 *Figure 9. Non-predictive model incorporating dual (fast+slow) control. The slow integrator can be added to predictive models*  
 755 *in the same way.*

756

757 With predictive control, there is an additional subtlety. In such systems, the fast integrator is  
 758 driven not by retinal defocus directly, but by the estimated future defocus (Figure 6). This does  
 759 *not* immediately drop to zero when pinholes are applied. When the system is made open-loop  
 760 by setting  $d(t)=a(t)$ , the input to the fast integrator becomes  $a(t-T_{sens})-a(t+T_{mot})$  for the no-  
 761 change prediction model. This becomes zero once accommodation has stabilised, but is finite  
 762 while it decays. When the gain of the slow integrator is sufficiently large, this small error input  
 763 is enough to keep the slow integrator high. This in turn keeps accommodation high and thus  
 764 sustains the error signal. Accommodation creeps slowly down to the rest focus with a time-  
 765 constant which, counter-intuitively, can be much longer than any of the three time-constants of  
 766 the system:  $\tau_{plant}$ ,  $\tau_{fast}$ ,  $\tau_{slow}$ . This effect is independent of exposure duration, so cannot account  
 767 for the adaptation which the slow integrator was introduced to explain. To avoid this effect and  
 768 obtain a clear difference between short and long exposure durations, we have found that  $G_{slow}$   
 769 needs to be less than around 10. Here, we have set  $G_{slow}=5$ .

770 The slow integrator also increases the overall steady-state gain and thus reduces the steady-  
 771 state error. Using Equation 15 and Equation 6, the steady-state accommodative response is

772

$$773 \quad a_{ss} = a_{RF} + \frac{G_{fast}(1 + G_{slow})}{1 + G_{fast}(1 + G_{slow})} (d_{ss} - a_{RF})$$

774

Equation 16

775 where with  $G_{fast}=8$ ,  $G_{slow}=5$  the gain term is 0.98, compared to 0.89 with only the fast  
776 integrator. Thus, following a step-change in demand, the model response rises rapidly to around  
777 90% of the demand, and then over the next tens of second rises more slowly to approach the  
778 demand exactly.

779 *Microfluctuations and noise*

780 Accommodation is subject to fluctuations, often called microfluctuations although they are  
781 actually quite substantial at around  $\pm 0.5D$ , exceeding the depth of field (Charman & Heron,  
782 1988, 2015). The source and purpose of these is unclear: they may represent neural noise,  
783 disturbances from the intraocular pulse, mechanical resonances within the ocular plant,  
784 deliberate attempts at “hunting” in order to find the best point of focus, and/or fluctuating input  
785 from the other influences on accommodation mentioned above (Charman & Heron, 1988,  
786 2015; Collins et al., 1995; Denieul, 1982; Gray et al., 1993b).

787

788 The power spectrum of open-loop accommodation is roughly a straight line on log-log axes  
789 (Campbell et al., 1959b; Campbell & Westheimer, 1960; Stark et al., 1965), i.e. a power-law  
790 spectrum,  $P=1/f^\alpha$ . We model this by injecting white noise onto the defocus signal prior to input  
791 to the neural controllers (Figure 11). White noise has a flat power spectrum, but integration by  
792 the two integrators within the system (the neural controller and the plant) converts it to a power-  
793 law spectrum, with an approximately Brownian ( $1/f^2$ ) spectrum.

794

795 Noise has often been omitted from models of accommodative control, presumably with the  
796 rationale that once the correct noise-free response has been obtained, noise can always be added  
797 later to simulate microfluctuations. However, this approach is unwise, because noise in fact  
798 adds important constraints to the system. This is especially true with a predictive control  
799 system, which can easily end up amplifying noise in the open-loop condition. Referring to  
800 Figure 6, we see that a predictive control system actually contains not one but two feedback  
801 loops: one via the eyes, and one internal to the brain, incorporating the virtual plant. Operating  
802 in open-loop mode cuts the outer feedback loop, but leaves the internal feedback loop intact.  
803 Depending on the coefficients, internal noise can easily resonate within this loop, creating a  
804 situation where the power spectrum of open-loop accommodation has sharp peaks which do  
805 not occur in closed-loop mode, since the outer feedback loop suppresses them in its effort to  
806 keep the error zero. This is not observed empirically. The power of low frequencies does  
807 increase in open-loop mode (Charman & Heron, 2015; Gray et al., 1993b), since without an

808 error signal accommodation performs a random walk around the rest focus, whereas it is kept  
809 close to the demand in closed-loop mode. But we do not see an increase in the power of  
810 particular high-frequencies, as would occur if internal noise were resonating within the internal  
811 feedback loop.

812

813 Fortunately, we find that the values we have already derived are consistent with these data. A  
814 more underdamped system – say  $G_{\text{fast}}=15$ ,  $\tau_{\text{fast}}=2\text{s}$ , which puts the damping coefficient  $\zeta$  at 0.5  
815 – does show unrealistic high-frequency resonances within the forward model feedback loop,  
816 but our sub-critically-damped parameters  $G_{\text{fast}}=8$ ,  $\tau_{\text{fast}}=2.5\text{s}$ ,  $\zeta=0.7$  already suppress the open-  
817 loop resonance.

818

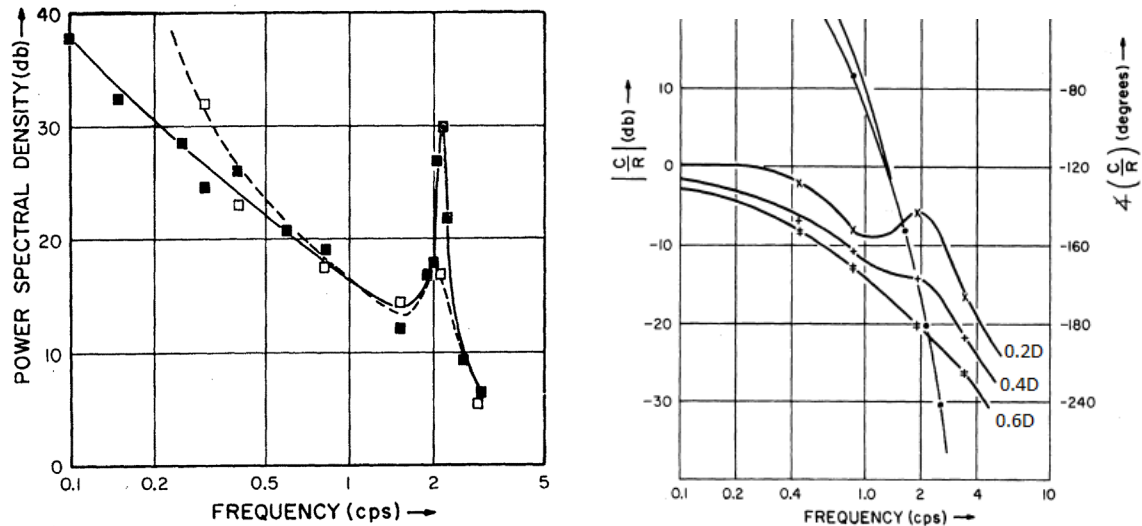
819 [Explaining the closed-loop resonance seen for high frequencies at low amplitudes](#)

820 In fact, several workers have found evidence for a resonance in closed-loop but *not* open-loop  
821 mode. The first evidence comes from microfluctuations during steady fixation. Several workers  
822 have found that the power-spectrum of closed-loop accommodation has a peak at around 2Hz  
823 (Figure 10A). It is not always present, but when found is always *more* prominent in closed-  
824 loop than open-loop accommodation. Although the location of this peak varies with heartrate,  
825 suggesting the pulse as a possible source interacting with blood volume of the ciliary body  
826 (Collins et al., 1995; Winn et al., 1990), the fact that it is higher in closed-loop conditions  
827 suggests that the source must be amplified by a neural resonance within the outer feedback  
828 loop.

829

830 Furthermore, the same resonance is assumed to be responsible for another puzzling  
831 observation, relating to gain with sinusoidal stimuli. In our discussion around Figure 8, we  
832 emphasised the lowpass nature of the gain response. This is true at high amplitudes, but for  
833 low-amplitude oscillations in demand, the curves become non-monotonic, with an increase in  
834 gain at around 2Hz (Figure 10B). Ockham's Razor suggests this reflects the same closed-loop  
835 resonance causing the ~2Hz peak in microfluctuations. However, the dependence on amplitude  
836 indicates that this resonance must be caused by a nonlinear mechanism, since for a linear  
837 system gain is independent of stimulus amplitude.

838



839

840

841

842

843

844

Figure 10. Evidence for a resonance at around 2Hz in accommodative control. (A) Figure 5 from Stark et al 1965 (Stark et al., 1965), replotting empirical results from Campbell et al 1959 (Campbell et al., 1959b), showing the power spectrum of accommodation under closed-loop (solid) and open-loop (pinhole, dashed) conditions. (B) Empirical results from Figure 4 of Stark et al 1965, showing gain for sinusoidal oscillations of three different amplitudes (0.2D, 0.4D, 0.6D). Gain is expressed in decibels (left axis): 0dB corresponds to an amplitude gain of 1, -10dB to 0.32, -20dB to 0.1, -30 to 0.03.

845

846

847

848

849

850

851

852

853

854

855

856

857

858

859

860

861

862

Resonances observed in closed- but not open-loop mode immediately suggest a control system lacking the predictor we have argued for so far. Non-predictive control is prone to closed-loop instabilities in systems with latencies, like accommodation. This occurs in the outer feedback loop via the eye, when the accommodation change designed to null out defocus arrives out of phase due to the latency and ends up enhancing the defocus which cause it. Predictive control avoids these closed-loop instabilities, but if the prediction is imperfect, it can be vulnerable to open-loop resonances due a similar effect occurring via the internal feedback loop driven by the efference copy. (For a mathematical justification of these statements, see the Appendix, specifically the discussion around Equation 17, Equation 18 and Equation 20.)

Thus to explain both the power spectrum of microfluctuations, and the non-linear resonance in the response to sinusoidal demand, we postulate an additional signal controlling accommodation. This is proportional to small amplitudes of the current defocus, not the estimated future defocus, and is thus not predictive. (This signal is, however, included within the efferent copy used to estimate future defocus within the predictive control system.) Because this signal is non-predictive, it is prone to closed-loop instabilities. But for the same reason, it avoids open-loop resonance which can occur within a predictive system.

863 To prevent the closed-loop instabilities from catastrophically destabilizing the response, we  
864 clip this non-predictive signal at a low value, set to 0.15D in our model (i.e. signals larger than  
865 0.15D in magnitude are set to  $\pm 0.15D$  depending on their sign). This saturating value is chosen  
866 simply because it gives a reasonable match to empirical results. It is low enough to ensure that  
867 the signal does not change the behavior of the model in response to large changes in defocus.  
868 However, it is large enough that the signal still produces a visible high-frequency peak in the  
869 power spectrum of closed-loop microfluctuations and a high-frequency resonance in the  
870 response to low-amplitude sinusoids (see Results).

871 This non-predictive saturating signal has other interesting effects on accommodation. Notably,  
872 it facilitates a rapid response to small step stimuli, because non-predictive proportional signals  
873 tend to react faster than predictive integral signals. For example, suppose demand suddenly  
874 increases by 0.1D, causing an 0.1D step-change in defocus. The non-predictive proportional  
875 control signal, with unit gain, requests the full 0.1D increase in accommodation. The fast  
876 integrator begins responding at the same time, but due to its integral nature, its response ramps  
877 up more gradually. Furthermore, because the non-predictive proportional signal uses the  
878 current sensed defocus, rather than the predicted future defocus, it stays requesting the full  
879 0.1D for at least 0.3s, until the sensorimotor latency has elapsed and the ocular plant starts to  
880 respond and thus reduces the sensed defocus. In contrast, input to the fast integrator is estimated  
881 future defocus, which begins to fall immediately based on the requested change to  
882 accommodation (the predictive control system assumes that demand will stay at the new value,  
883 but it predicts that defocus will fall because of the predicted accommodative response). So, the  
884 input to the fast integrator begins to fall immediately from its initial peak of 0.1D, whereas the  
885 input to the proportional controller stays at 0.1D until the sensorimotor latency has elapsed.  
886 Thus for small step-changes in defocus, the non-predictive proportional signal enables a larger,  
887 faster response. However, the saturation means that its effect is limited to small changes, with  
888 the predictive-integral control dominating the response to large changes. Dynamics of larger  
889 step responses are controlled with a pulse signal (Bharadwaj & Schor, 2005, 2006; Schor &  
890 Bharadwaj, 2006, 2004) that will be added to this model in a subsequent paper.

891

892 Depth of focus

893 In principle, small enough changes in defocus that, given the eye's optics, produce no  
894 significant change in the retinal image cannot drive accommodation. The smallest change in

895 defocus which produces a detectable change in accommodation is referred to as objective depth  
896 of focus. This is typically much smaller than the subjective depth of focus, i.e. the smallest  
897 change in defocus which produces a perceptible change in image quality (Kotulak & Schor,  
898 1986a; Udlam et al., 1968; Yao et al., 2010). Depth of focus is often modelled as a deadzone  
899 (e.g. (Schor, 1979b)): the defocus signal is set to zero unless it exceeds some threshold value  
900 corresponding to the objective depth of focus, say 0.2D. However, this approach has a number  
901 of drawbacks:

902 (i) It can result in unrealistic jumps, where a small change in demand pushes the defocus above  
903 the threshold and thus elicits a disproportionately large response.

904 (ii) It produces a hysteresis effect, whereby accommodative lead and lag can depend on how  
905 the demand is approached. For example, with a threshold of 0.2D, if the demand steps up from  
906 1D to 2D, the effective defocus becomes zero once accommodation reaches 1.8D, so we get a  
907 lag. But if demand steps down from 3D to 2D, effective defocus becomes zero once  
908 accommodation reaches 2.2D, so we get a lead. This hysteresis is not typically observed, except  
909 with extremely blurred images (Heath, 1956a) .

910 (iii) It reduces the gain of the response to low-amplitude oscillations. For example, consider a  
911 slow oscillation ranging between 1D and 3D. Assume for simplicity that the closed-loop gain  
912 of the system is 1, so that in the absence of a deadzone, the response would track demand  
913 exactly. With a deadzone clipped at 0.2D, the response would range from 1.2D to 2.8D,  
914 reducing the gain to 0.8. With a lower-amplitude oscillation where demand ranged from 1.5D  
915 to 2.5D, the response would range from 1.7D to 2.3D, making the gain 0.6. With a still lower-  
916 amplitude demand ranging from 1.7D to 2.3D, response would range from 1.9D to 2.1D,  
917 making the gain 0.3. Yet this decrease in gain with decreasing amplitude is not observed. In  
918 fact, accommodative gain tends to be smallest for high amplitudes, not for low amplitudes  
919 (Stark et al., 1965, p. 196).

920

921 For all these reasons, we have chosen not to include a dedicated defocus deadzone in our model.  
922 The objective depth of focus is adequately accounted for by the white noise we have added to  
923 the defocus signal, which effectively swamps small changes.

924

925

926

## 927 [Simulink implementation and summary of the model](#)

928 Figure 11 shows the complete model as it appears in our Matlab Simulink implementation,  
929 incorporating all the elements discussed above. The model has two inputs: (1) “demand”,  
930 accommodative demand in diopters, and (2) “pinhole”, which conveys whether the eye is  
931 currently viewing through a pinhole or not. If pinholes are present, the defocus signal is set to  
932 zero; otherwise it is set to demand minus accommodation. The defocus signal has white noise  
933 added to it and is delayed by the sensory latency before reaching the “brain” module.

934

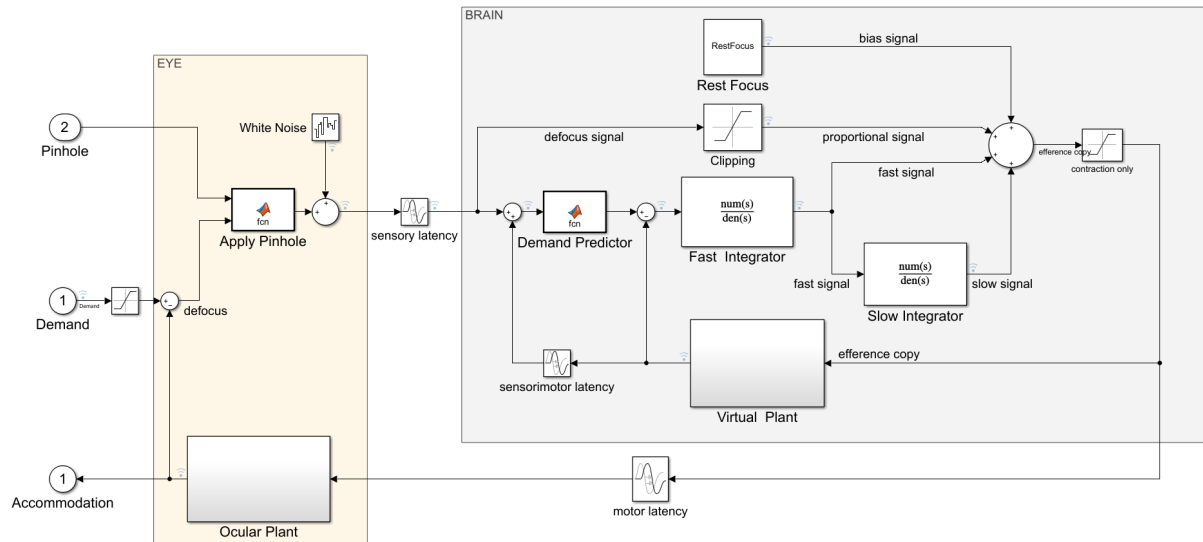
935 Here, four signals are combined to produce a neural signal which is delayed by the motor  
936 latency before reaching the ocular plant. From top to bottom, these four signals are: (1) the  
937 constant bias signal, which sets the rest focus; (2) the proportional signal, which is simply the  
938 noisy defocus signal clipped at  $\pm 0.15D$ ; (3) the signal from the fast integrator, which is driven  
939 by the estimated future defocus; (4) the signal from the slow integrator, which is driven by the  
940 fast integrator. One final detail not mentioned so far is that the neural signal is thresholded at  
941 zero to ensure it is positive. This is visible in the diagram as the “saturation” block on the far  
942 right, immediately after the four signals are combined. This accounts for the fact that the ciliary  
943 muscle can only be commanded to contract, making the lens more convergent, or allowed to  
944 relax. Negative values would effectively command the ocular lens to adopt a divergent form,  
945 which is physically impossible.

946

947 As well as being sent down cranial nerve III to the eye, an efferent copy of the neural signal is  
948 directed to a virtual plant within the brain, which predicts the future accommodation. This in  
949 turn is used to estimate the future defocus which drives the fast integrator. For completeness,  
950 we have included a block labelled “Demand Predictor”, although in the current instantiation of  
951 the model, this simply passes its input through unchanged.

952





953

954

Figure 11. Simulink block diagram of our final model, incorporating all the features discussed in the paper. The Simulink model has two inputs: (1) demand, and (2) whether or not the eye is viewing through a pinhole. It has one output: accommodation.

956

957

#### 958 Simulation details

959

The next section shows simulation results for sine and step stimuli with this model. All simulations were run in Simulink, Matlab R2020b, with a variable-step solver, automatic solver selection and the default settings (relative tolerance 0.001 and max/min/initial step size and absolute tolerance all set to “auto”). For plotting, we interpolated the output to obtain results every millisecond. Note that this can give the impression of greater variability than in some empirical results where accommodation may be measured at a much lower rate, e.g. 50Hz. To obtain the velocity traces shown in Figure 17, we took the difference between successive accommodation values to obtain the change per millisecond, then smoothed this within a moving window of 10ms.

968

969

To obtain the model gain and phase in response to sinusoidal oscillations in demand, we ran the model for 25 cycles of the specified frequency, then fitted a sinewave to the results using Matlab’s Curve Fitting Toolbox. We fixed the frequency of the sinewave to the frequency of the stimulus and fitted the three free parameters baseline, amplitude and phase (see code in Run\_Sine.m). The amplitude and phase of the response were taken to be those of the fitted sinewave.

975

976 The simulation shows onset transients at its start point, as the integrators settle. In all cases, we  
977 therefore discarded the first few seconds of simulation time in order to exclude these transients.  
978

## 979 Results

980 The different elements of this model were motivated by different observations – the gain and  
981 phase to sinusoids; adaptation; power spectra of microfluctuations so on. Components such as  
982 the fast and slow integrator and the virtual plant have been proposed before for the  
983 accommodation step response (Schor & Bharadwaj, 2005), but to our knowledge never tested  
984 in combination for pursuit sinusoidal tracking (Schor & Kotulak, 1986) or adaptation (Schor,  
985 1979b), or with white noise and the feeding through of a clipped signal proportional to the  
986 current defocus. This combination is to our knowledge a novel contribution. We now  
987 demonstrate that this unified model can reproduce each of the observations that motivated its  
988 different components.

989

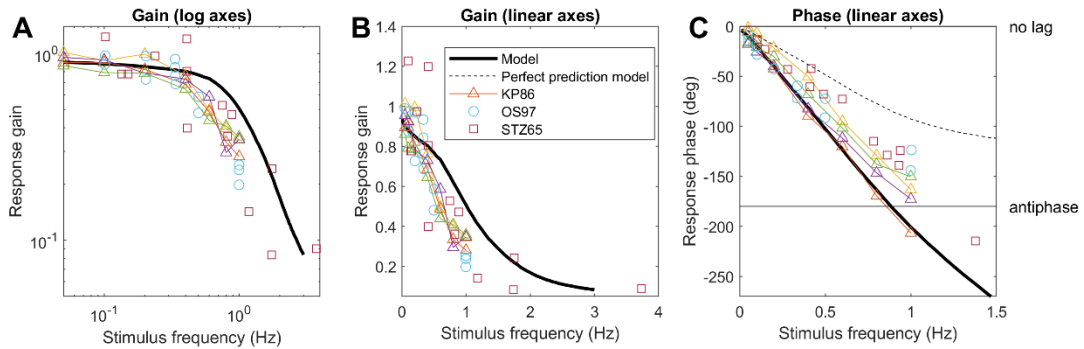
### 990 Response to sinusoidal demand

991 Figure 12 shows the gain and phase of the model (heavy black line), compared with results  
992 from human subjects digitised from (Kruger & Pola, 1986; Ohtsuka & Sawa, 1997). This is of  
993 course similar to results already shown in Figure 8, but whereas those curves were obtained  
994 from mathematical formulae for a leaky integrator in a predictive control system, Figure 12 is  
995 obtained via Simulink simulation of the full four-signal model with noise. There is reasonable  
996 agreement in gain (Figure 12AB); both humans and model are low-pass. The main quantitative  
997 disagreement is that the “knee”, where the gain drops rapidly, typically occurs around 0.4Hz  
998 in humans and slightly later, around 0.6Hz, in the model. There is also good agreement in phase  
999 (Figure 12C). For comparison, the dashed black line shows the phase which would be obtained  
1000 for a model with perfect demand prediction. As we showed above, this can be obtained from  
1001 the phase of our model with “no change” demand prediction by subtracting the sensorimotor  
1002 latency:  $\phi_{\text{perfect}} = \phi_{\text{nochange}} - 360fT_{\text{sens}}$ . Interestingly, the phase function of most human subjects  
1003 agrees better with that of the no-change model rather than the perfect model, suggesting that  
1004 these subjects had little ability to predict the oscillatory demand.

1005

1006

1007



1008

1009

1010

1011

1012

1013

1014

1015

1016

1017

Figure 12. Gain and phase of the model response to sinusoidal demand, compared to empirical results. A,B: Gain plotted on linear and log axes. C: Phase plotted on linear axes. The heavy black line is the response of the model in Figure 11 with the parameters given in Table 2. The dashed black phase line shows the phase which would be obtained by a model capable of perfectly predicting the sinusoidal oscillation in demand. Triangles show empirical results for four human subjects, digitised from Kruger and Pola (Kruger & Pola, 1986), using the data with white light and defocus cue only. Circles are for a further four subjects, digitised from Ohtsuka and Sawa (Ohtsuka & Sawa, 1997), using only their control subjects. In (Kruger & Pola, 1986) and in the model, the demand oscillated between 1D and 3D, i.e. the amplitude of the sinusoid was 1D and its mean value was 2D. In (Ohtsuka & Sawa, 1997), the amplitude was 1.5D and its mean value is not stated. Code to generate this figure is in Fig\_CompareGainPhase.m. Run\_Sine.m must be run first to generate the model data.

1018

1019

1020

1021

1022

1023

1024

1025

1026

1027

1028

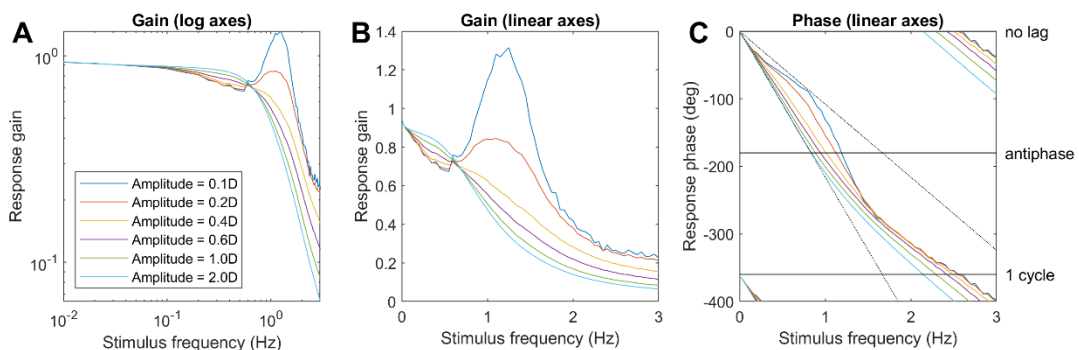
1029

Figure 12 was for sinusoidal demand oscillations with an amplitude of 1D. Of course, the gain and phase of a linear system are independent of amplitude. However, our model is nonlinear due to the saturation of the non-predictive proportional signal. Figure 13 shows the gain and phase in the same format as Figure 12, but for different amplitudes of oscillation around a 2D baseline. The green lines are for the 1D amplitude shown in Figure 12, but for lower amplitudes the gain and phase start to deviate significantly from these results. Most strikingly, there is a resonance at 1.2Hz where the gain actually goes above 1 for the smallest oscillations ( $\pm 0.1D$ ). This represents the instability caused by the non-predictive proportional signal. Since this signal is clipped at  $\pm 0.15D$ , it has a significant effect only for low-amplitude oscillations.

1030

1031

1032



1033

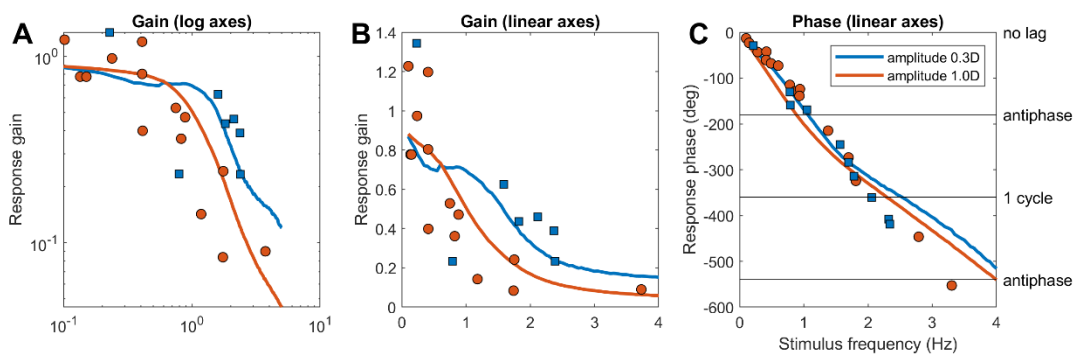
1031 *Figure 13. Model gain and phase as a function of amplitude. The green curves (1D) are what was shown in Figure 12, but we*  
1032 *see that the behaviour at low amplitudes is quite different, with a resonance at 1.2Hz. Code to generate this figure is in*  
1033 *Fig\_Sine.m. Run\_Sine.m must be run first to generate the model data.*

1034

1035 This effect is qualitatively in agreement with the low-frequency resonance reported by Stark et  
1036 al. (Stark et al., 1965), which led them to conclude that human accommodative control must  
1037 include a nonlinearity. Digitized data from (Stark et al., 1965) is replotted in Figure 14, along  
1038 with the response of the model. The model does not reproduce the strong dip in gain at 0.8Hz  
1039 for an amplitude of 0.3D, but apart from that, the agreement is quite good. In particular, it  
1040 accounts for the key observation that gain is quite high, around 0.5, for 0.3D-amplitude  
1041 oscillations at around 2Hz, whereas gain is much lower, around 0.1, for higher amplitude  
1042 oscillations at this frequency.

1043

1044



1045

1046 *Figure 14. Symbols are digitised data from Figure 3 of Stark, Takahashi & Zames (Stark et al., 1965). These are measured*  
1047 *gain and phase for one subject, for amplitudes of 0.3D (blue) and 1D (orange). The curves are model gains and phase for*  
1048 *these amplitudes, about a baseline of 2D. Code to generate this figure is in Fig\_StarkTakahashiZames.m.*  
1049 *Run\_StarkTakahashiZames.m must be run first to generate the model data.*

1050

### 1051 Limiting tracking frequency

1052 Figure 13C and Figure 14C showed that the phase of the response relative to demand increases  
1053 with frequency, reaching 180 degrees at a frequency of around 1Hz. When this occurs, the  
1054 demand and response are in antiphase, and the error is greater than the stimulus. Interestingly,  
1055 if the response gain were zero, then the error for the 180 deg phase delay would be smaller than  
1056 if the gain were 1.0. It is therefore of interest to ask how the gain and phase changes affect  
1057 defocus error for demand oscillations of different amplitude and frequency. We quantify this  
1058 using the mean absolute defocus error. The defocus error is the difference between demand and

1059 accommodation at any time; absolute defocus error is the rectified version of this waveform,  
1060 and mean absolute defocus is the average value of this over time:  $\langle |d(t) - a(t)| \rangle$ , where  
1061  $d(t) = D_{mean} + D_{amp}(\sin 2\pi ft)$ .

1062  
1063 The heavy curves in Figure 15A show how mean absolute defocus error varies with amplitude  
1064 and frequency of sinusoidal demand. In each case, the peak error is just below 1Hz, when the  
1065 response is 180° out of phase with the demand (Figure 13C). The error increases with demand  
1066 amplitude, even though for frequencies below the peak, the gain (i.e. the ratio of response to  
1067 demand) is closer to 1 for larger amplitudes (Figure 13AB).

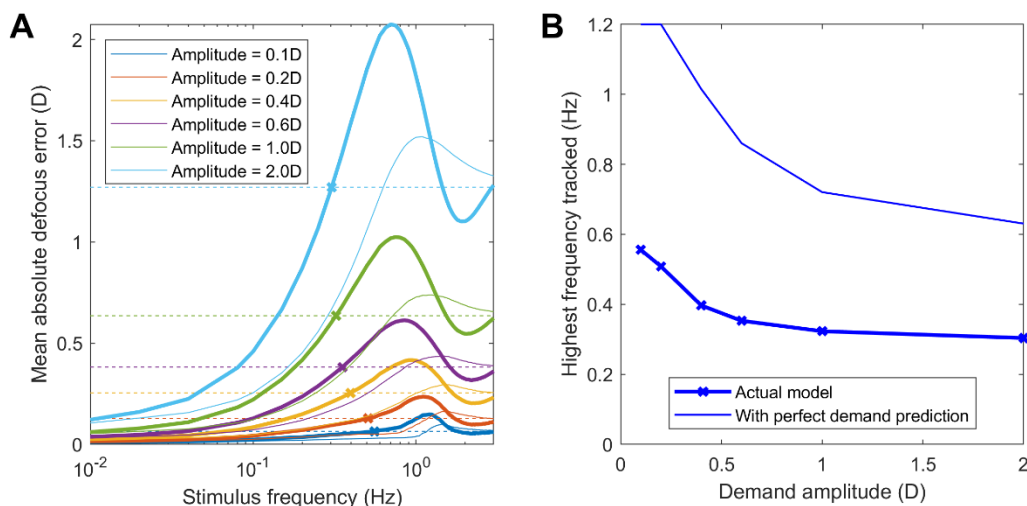
1068  
1069 The aim of accommodative control is to track demand so as to minimize defocus error,  
1070 but the phase-delay means that for sufficiently high frequencies, this aim would be better  
1071 achieved by simply keeping accommodation fixed at the mean demand, i.e. by having a  
1072 response gain of 0, rather than attempting to track oscillations in demand about this baseline.  
1073 The dashed lines in Figure 15A shows this *zero-gain tracking error*, i.e. the mean absolute  
1074 defocus error which would be achieved if accommodation stayed at the steady-state value  
1075 elicited by the mean demand ( $D_{mean}=2D$  in this example). Because the amplitude of zero gain  
1076 tracking error depends only on the input amplitude, the error is independent of temporal  
1077 frequency of the sine input. Since the static accommodative lag is small, the zero-gain steady-  
1078 state response is also close to  $2D$ . So the mean zero-gain error is approximately the average  
1079 value of  $|D_{amp}(\sin 2\pi ft)|$ , or  $2D_{amp}/\pi$ , where  $D_{amp}$  is the amplitude of the demand oscillations  
1080 about the  $2D$  baseline.

1081  
1082 We define the *limiting tracking frequency* to be the frequency at which the actual gain  
1083 and phase-delay of the accommodative response produces the same error as would be achieved  
1084 with zero gain. This is where the zero-gain tracking error is first equal to the actual error,  
1085 marked with a cross x in Figure 15A. For frequencies lower than this limit, the oscillation in  
1086 accommodative response is helpful, i.e. it tracks the oscillations in demand with a phase delay  
1087 low enough to reduce the mean defocus error below the zero-gain tracking error. However for  
1088 frequencies above the limit marked with a cross, the oscillatory response is out of phase and  
1089 ends up making mean defocus error larger than if accommodation simply remained constant at  
1090 the baseline value.

1091

1092 Because of the nonlinearity represented by the saturating non-predictive proportional  
1093 signal, this limiting-tracking frequency depends on amplitude, as shown in Figure 15B. For  
1094 large-amplitude oscillations in demand, accommodation can track only up to around 0.4Hz.  
1095 We saw above that the non-predictive proportional signal enables a more rapid response to  
1096 small changes. This is shown in Figure 15B by the increase in limiting tracking frequency for  
1097 low-amplitude oscillations.

1098  
1099 Using the result that perfect demand prediction would reduce the phase by the sensorimotor  
1100 latency, we can also infer what these curves would be for a model with perfect demand  
1101 prediction but with the same leaky-integral controller. These are shown with the light curves  
1102 in Figure 15AB. Perfect demand prediction does reduce the error and increase the limiting  
1103 tracking frequency, but not dramatically, because of limits imposed by the time constant of the  
1104 plant and the fast integrator.



1105  
1106 *Figure 15. (A) Mean absolute defocus error for sinusoidal demand oscillations of different frequencies and amplitudes about*  
1107 *a 2D baseline. The heavy curves show  $|d(t)-a(t)|$  for our model with its observed gain and phase; the light curves are those*  
1108 *inferred for a model with perfect demand prediction. The dashed lines show the expected high-frequency limit, i.e. the mean*  
1109 *defocus error if the demand oscillated but the response stayed at the steady-state value elicited by the mean demand, and*  
1110 *the crosses indicate where this is first less than the error with tracking. The crosses mark where this crosses the mean defocus*  
1111 *error. We take this as an indication of the highest frequency which can be successfully tracked at this amplitude. (B) Tracking*  
1112 *frequency limit as a function of amplitude, for the actual model (heavy line, crosses) and for a model with perfect demand*  
1113 *prediction (upper light line). Code to generate this figure is in Fig\_Sine.m. Run\_Sine.m must be run first to generate the model*  
1114 *data.*

1115

### 1116 Steady-state microfluctuations

1117 Figure 16A shows example closed- and open-loop accommodation traces recorded from the  
1118 model over the course of 5 minutes. The red trace is for closed-loop viewing of a stimulus at  
1119 1D (red dashed line). Accommodation thus fluctuates around a value a little over 1D, reflecting  
1120 the accommodative lead for a stimulus nearer than the rest focus, here 1.4D. The fluctuations  
1121 span a range of around 0.1D ( $\pm 2SD$ ). The SD is 0.03D, which is small compared to the SD of  
1122 human microfluctuations (0.1-0.3D, (Charman & Heron, 1988, 2015; Gamba et al., 2009)).  
1123 The power spectrum, Figure 16D, has a prominent peak at around 1.5Hz. This periodic  
1124 structure is clearly visible in the 10s except from the trace shown in Figure 16B.

1125

1126 The blue trace is for open-loop viewing, e.g. through pinholes. Now, the response wanders  
1127 around the rest focus, 1.4D (dashed blue line). However, because the bias is constant rather  
1128 than scaling with the difference between accommodation and rest focus, the excursions are  
1129 much wider. This is visible in the power spectrum, Figure 16D, where the power continues to  
1130 rise as frequency reduces.

1131

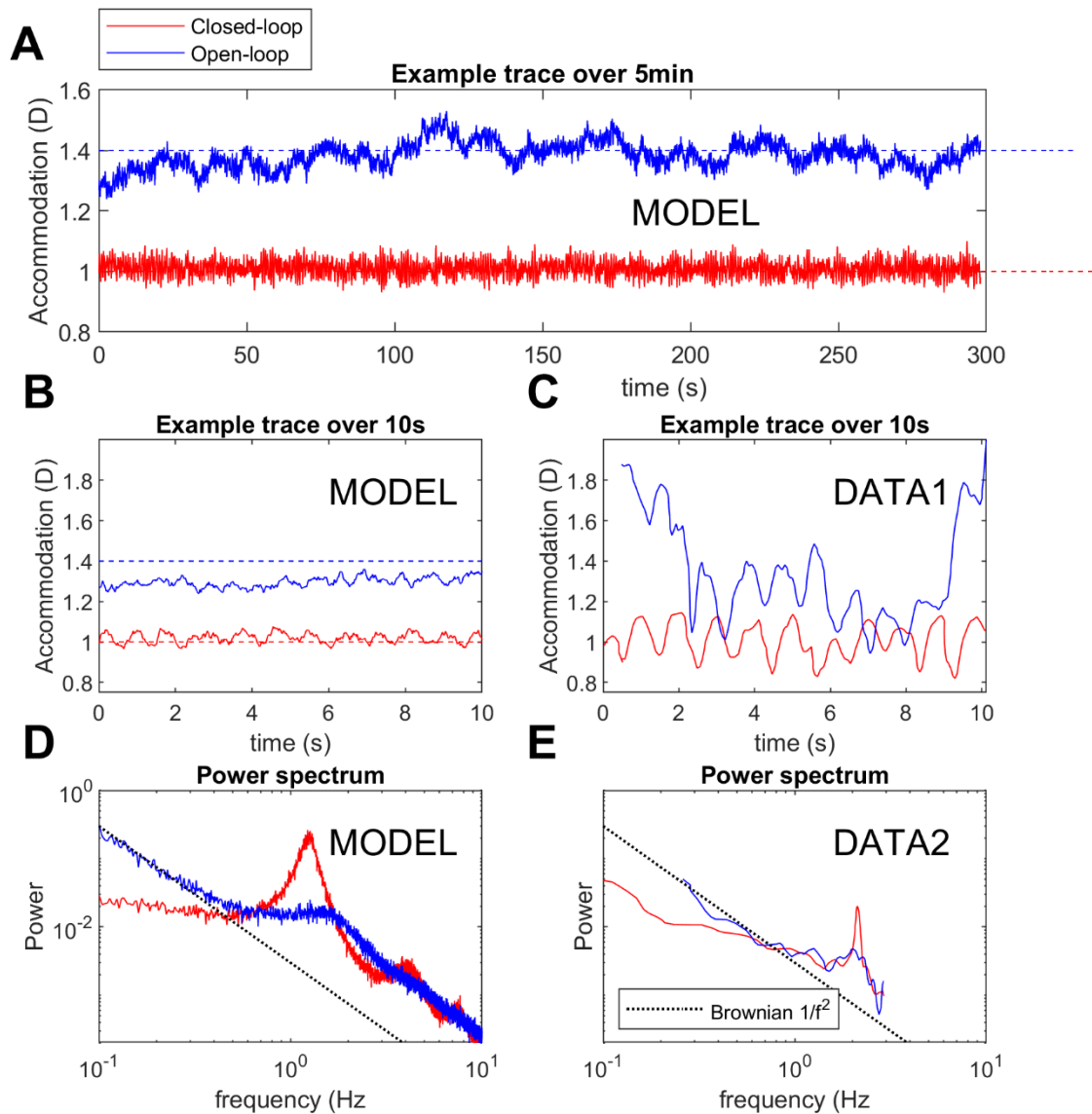
1132 Figure 16B shows a 10s excerpt from the trace in Figure 16A, for comparison with the example  
1133 empirical data in Figure 16C, digitized from (Gray et al., 1993a). Although the amplitude of  
1134 the microfluctuations is larger in the human observer, the same qualitative features are visible:  
1135 closed-loop mode showing strong periodic structure at around 2Hz, open-loop mode showing  
1136 much larger low-frequency fluctuations. Figure 16E shows the closed- and open-loop power  
1137 spectra for a human observer, digitized from (Campbell et al., 1959b), for comparison with  
1138 Figure 16D.

1139

1140 The presence of this relatively large, 1-2Hz periodic component in the closed-loop  
1141 microfluctuations may aid accommodative control, for example by “hunting” for the point of  
1142 optimal focus (Kotulak & Schor, 1986c). Thus, this could be a reason why the postulated non-  
1143 predictive proportional signal is beneficial for accommodative control.

1144

1145



1146  
 1147 *Figure 16. AB: Example accommodation traces in (red) closed-loop response to 1D and (blue) open-loop mode. Dashed*  
 1148 *horizontal lines show (red) the 1D demand and (blue) the 1.4D rest focus. A: trace over 5 minutes, to show slow fluctuations*  
 1149 *in open-loop response; B: 10s excerpt from A, to facilitate comparison with C: Example 10s trace recorded from a human*  
 1150 *observer, digitised from Fig 3 of Gray, Winn and Gilmartin (Gray et al., 1993a). The red trace is for a 5mm pupil; the blue trace*  
 1151 *is for viewing through pinholes of 0.5mm diameter. A scalebar but no accommodation values are provided in (Gray et al.,*  
 1152 *1993a), so the vertical position is arbitrary. To facilitate comparison with the model, we have set the mean value to 1D for*  
 1153 *the closed-loop and 1.4D for the open-loop trace. D: Power spectra of the closed- and open-loop response, obtained by*  
 1154 *averaging the Fourier power spectra of 50 traces like those in A, generated from simulations with different noise seeds. For*  
 1155 *comparison, a  $1/f^2$  Brownian noise spectrum is drawn on with a black dashed line. E: Power spectra of closed- and open-loop*  
 1156 *responses for a human observer, digitised from Fig 5 of (Campbell et al., 1959b). This is labelled DATA2 to make clear that it*  
 1157 *is not the power spectrum of the trace shown in Figure 16C. No vertical axis scale was provided in (Campbell et al., 1959b),*  
 1158 *so we have scaled the spectrum so it best agrees with D. The red curve was recorded with a 7mm pupil and the blue curve*  
 1159 *with a 1mm effective entrance pupil. Code to generate this figure is in Fig\_Noise.m; Run\_Noise.m must be run first to generate*  
 1160 *the data.*



1161

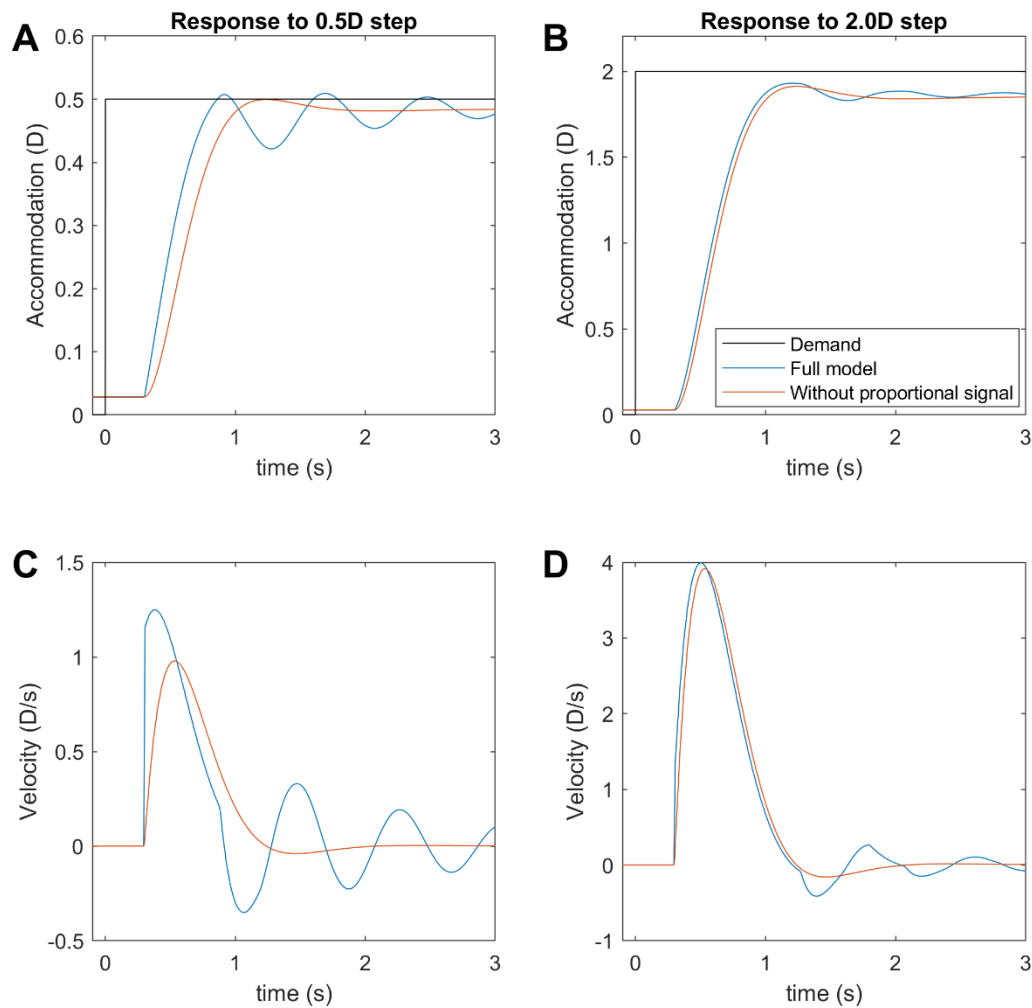
1162

### 1163 [Response to step changes](#)

1164 When motivating the introduction of the saturating non-predictive proportional signal, i.e. a  
1165 proportional controller responding to the current defocus signal (Figure 11), we discussed why  
1166 it produces a larger, more rapid response to small changes in demand. We have already seen  
1167 how this effect produces a higher gain for high-frequency low-amplitude oscillations (Figure  
1168 13) and thus the ability to track low-amplitude oscillations out to higher temporal frequencies  
1169 than is possible for larger amplitudes (Figure 15). Similarly, the non-predictive proportional  
1170 signal, clipped at  $\pm 0.15D$ , enables a faster response to small step changes in demand.

1171

1172 Figure 17 demonstrates this by comparing results from the full model (blue) with those from a  
1173 model identical except that it lacks the non-predictive proportional signal (orange). To enable  
1174 the effects to be seen clearly, noise is also turned off in this simulation. On the left, Figure  
1175 17AC, we plot the accommodation and velocity for a 0.5D increase in demand. The model with  
1176 the non-predictive proportional signal responds more quickly. We also see the characteristic  
1177 ringing, which is of course what drives the high-frequency peak in the microfluctuations.  
1178 However, for the larger 2D step shown on the right (note different y-scales), the saturation of  
1179 the non-predictive proportional signal at 0.15D limits its effect, and it makes barely any  
1180 difference either to accommodation itself or to velocity. In fact, for large step changes like that  
1181 shown in Figure 17BD, there appears to be a fifth signal, a nonlinear pulse triggered by sudden  
1182 large changes in demand (Schor & Bharadwaj, 2006, 2004). The pulse accounts for the  
1183 empirical observation that the peak acceleration of the response for step increases in demand  
1184 is roughly independent of the step size, instead of scaling with step size as would occur for a  
1185 linear system. While implementing the pulse is beyond the scope of this paper, we note that the  
1186 non-predictive proportional signal already moves in the right direction by boosting the  
1187 acceleration for small steps, and thus helping reduce the difference between acceleration for  
1188 large and small steps. This could be another reason for the accommodative control system to  
1189 include the postulated non-predictive proportional signal.



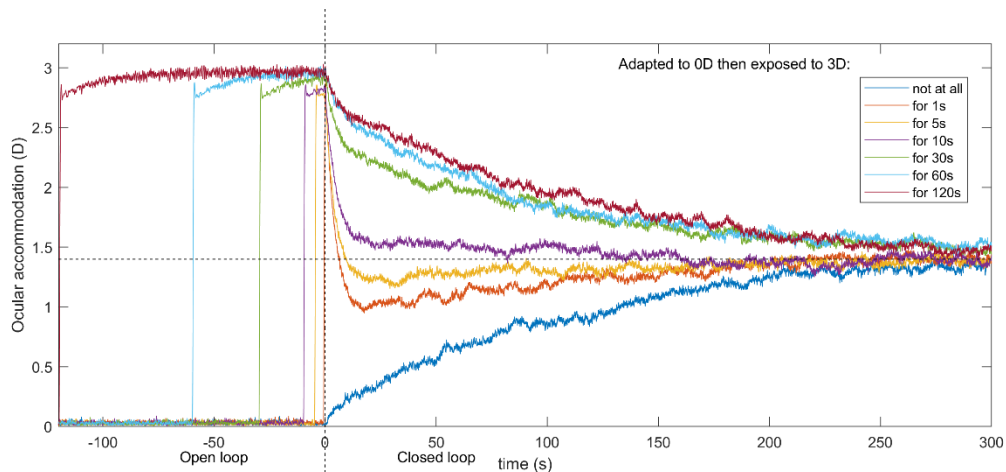
1190  
1191 *Figure 17. Noise-free accommodation (AB) and velocity (CD) for two different step increases in demand (AC: 0.5D, BD: 2D).*  
1192 *The blue curve is for the usual model; the orange curve is for a similar model with no non-predictive proportional signal. To*  
1193 *enable the effect to be seen clearly, noise has been turned off for this figure only. Also note that the response to the 2D step*  
1194 *(BD) is included only to demonstrate the role of the non-predictive proportional signal. The model presented in this paper*  
1195 *does not accurately capture the dynamics of the response to such large steps, since it does not include the pulse signal (see*  
1196 *text). Code to generate this figure is in Fig\_EffectOfPropSignal.m.*

1197

## 1198 Adaptation

1199 Next, we examine how the model adapts to accommodative demand to which it is exposed for  
1200 more than a few tens of seconds. This was the motivation for postulating the slow integrator  
1201 (Schor, 1979b; Schor et al., 1986). Its presence has not contributed to the results presented so  
1202 far, other than to boost the gain for very slow oscillations. Now we see how it accounts for  
1203 adaptation.

1204 Figure 18 shows the time course of accommodation following the application of pinholes at  
1205  $t=0$ , shifting the system from closed-loop to open-loop demand. After the application of  
1206 pinholes, accommodation eventually ends up at the rest focus, but how rapidly it does so  
1207 depends on the demand before pinholes were applied. The model observer is initially adapted  
1208 to 0D, then switches to viewing 3D for variable amounts of time as shown in the legend. The  
1209 results show that after viewing one demand for at least two minutes, the observer adapts to it  
1210 such that accommodation remains close to the adapted value for several minutes after pinholes  
1211 have been applied (uppermost/red, lowermost/blue traces). Conversely, when the observer was  
1212 exposed to different demands immediately before pinholes are applied (middle traces), they  
1213 move much more rapidly to the rest focus.  
1214



1215  
1216 *Figure 18. The model shows adaptation to demand, due to the slow integrator. The model observer is initially viewing an*  
1217 *object at 0D, before then viewing an object at 3D for varying durations as shown in the legend. Pinholes are applied at  $t=0$ ,*  
1218 *putting the system in open-loop mode. After long exposures, accommodation adapts to the demand, and moves only slowly*  
1219 *to the rest focus; the adaptation affects the accommodation for many minutes after pinholes have been applied (e.g. dark*  
1220 *blue curve: adapted to 0D, further than rest focus; red curve: adapted to 3D, closer than rest). Code to generate this figure is*  
1221 *in Fig\_Adaptation.m; Run\_Adaptation.m must be run first to save the data in Results\_Adaptation.mat.*

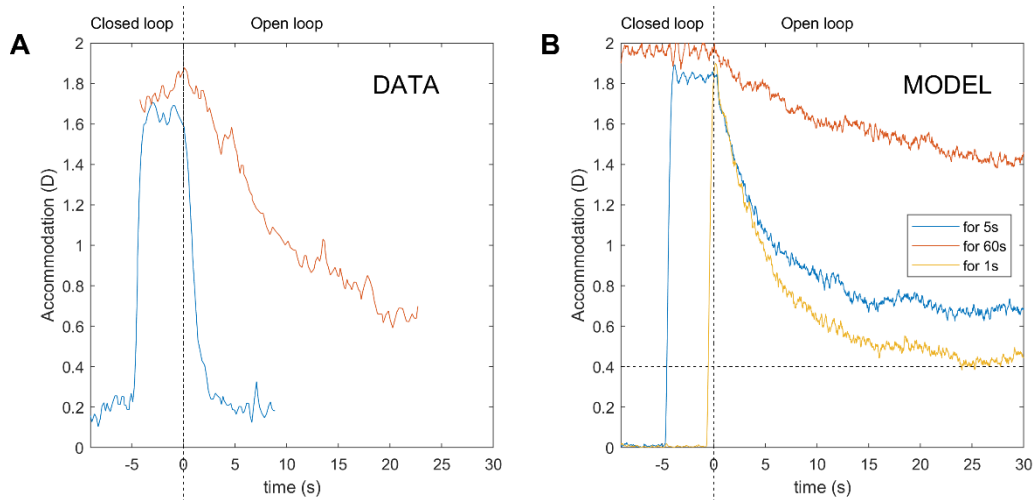
1222

1223

1224

1225 Figure 19 shows a comparison with empirical data. Here, the observer was exposed to a demand  
1226 of 2D for either 5s (blue) or 60s (orange) before moving to open-loop mode at  $t=0$ . The traces  
1227 in Figure 19A are for a human observer (Schor et al., 1986); those in Figure 19B are from the  
1228 model, with rest focus set to 0.4D (dashed line) in order to better match this observer. In both

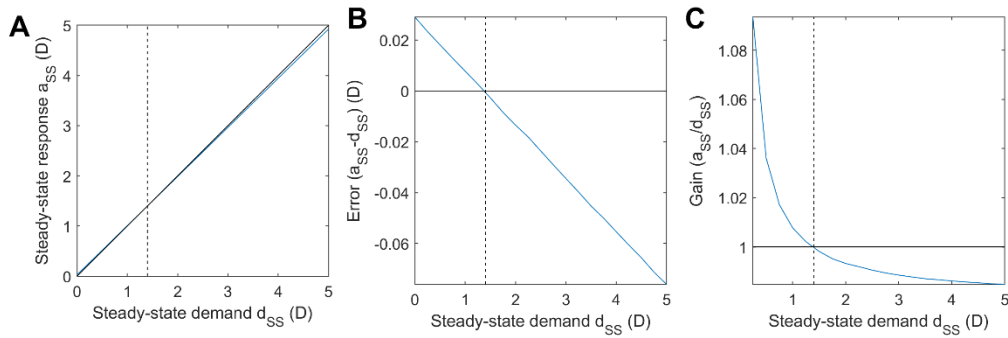
1229 cases, following the 5s exposure to 2D, accommodation falls rapidly once the system enters  
1230 open-loop mode, but following the 60s exposure, the decay is much slower.  
1231



1232  
1233 *Figure 19. Comparison of the model (B) with data digitised from Schor, Kotulak & Tsuetaki (Schor et al., 1986) (Fig 2, empty*  
1234 *field condition). As in Figure 18, pinholes are applied at t=0. Before then, the demand is at 0D for a long period, before moving*  
1235 *to 2D for either 5s (blue) or 60s (orange); for the model, we also include 1s (yellow). In (Schor et al., 1986), a scalebar is*  
1236 *provided, but absolute dioptre values are not available. The vertical position in the DATA panel is therefore arbitrary.*  
1237 *However, since the open-loop condition decays by well over 1D from the closed-loop position adopted in response to a 2D*  
1238 *demand, it seems clear that the rest focus for this observer was well below 1.4D. For this comparison, therefore, the rest*  
1239 *focus of the model has been set to 0.4D (dashed line) in this figure only. Code to generate this figure is in*  
1240 *Fig\_SchorKotulakTsuetaki.m.*

1241  
1242 **Steady state error**

1243 Finally, Figure 20 shows the model's steady-state error. As discussed (Equation 16), this  
1244 reflects both the fast and slow integrator. In the model, the additional gain provided by the slow  
1245 integrator means that steady-state error eventually becomes extremely small. Figure 21 shows  
1246 this process for an example step up to 2D. The error is zero at the resting focus but shows  
1247 lag/lead on either side of this. The gain (response/demand) therefore becomes high as demand  
1248 tends to zero.  
1249



1250

1251

1252

1253

1254

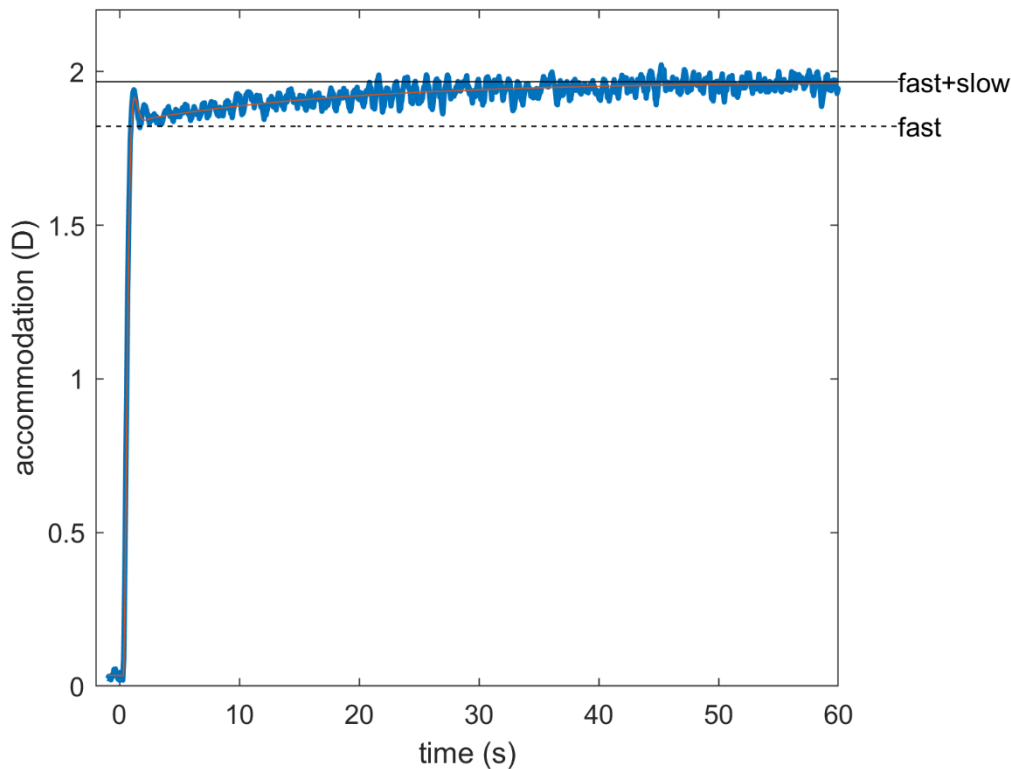
1255

1256

1257

Figure 20. Steady-state response of the model. The model was run for 320s with a constant demand  $d_{SS}$  indicated by the value on the x-axis, and accommodation was averaged over the final 60s to obtain the steady-state response,  $a_{SS}$ . (A) Input/output function, i.e. steady-state accommodation as a function of demand. (B) Steady-state error, i.e. difference between response and demand. For distant stimuli, this is positive (lead); for near, it is negative (lag). (C): Gain, i.e. ratio of response to demand. In each case, blue curves show the response of the model; solid black line indicates response equal to demand, and the dashed vertical line marks the rest focus, where this occurs. Code to generate this figure is in `Fig_SteadyState.m`; `Run_SteadyState.m` must be run first to save the data in `Results_SteadyState.mat`.

1258



1259

1260

1261

1262

1263

Figure 21. Model response to a step change in demand from 0D to 2D, showing the immediate rise to 89% of demand due to the fast integrator, and the subsequent slow rise to 98% demand due to the slow integrator. The blue trace is one example run from the full model; the superimposed orange line shows the response with no noise or non-predictive proportional signal, in order to isolate the response due to the fast and slow integrators. Note that the dynamics of the immediate response to

1264 *the step are not correct because they do not incorporate the pulse signal, but the point of this figure is to demonstrate the*  
1265 *time-course following this immediate response. Code to generate this figure is in Fig\_ExampleStep.m*

1266

## 1267 Discussion

1268 In this paper, we have discussed the neural control of accommodation. We have provided a  
1269 tutorial overview of the relevant control theory and key empirical observations. We have  
1270 discussed the evidence for a predictive control system, i.e. one incorporating a forward model  
1271 to predict the accommodative response in advance of the motor latency (Hung et al., 2002;  
1272 Khosroyani & Hung, 2002; Schor & Bharadwaj, 2004). Our analysis has led us to make the  
1273 novel proposal that a saturating non-predictive proportional-control component may operate in  
1274 parallel to the main predictive integrative-control feedback loop. This non-predictive  
1275 proportional signal causes a high-frequency resonance in the closed-loop response, observed  
1276 in the response to low-amplitude sinusoidal oscillations in demand. It amplifies noise within  
1277 the system, explaining the high-frequency peak observed in closed-loop but not open-loop  
1278 accommodation microfluctuations. It also speeds up the response to small, sudden changes in  
1279 demand. Yet its saturation means that it does not destabilize the system as a whole, and that it  
1280 becomes insignificant for large changes in demand.

1281

1282 We have implemented these ideas in a Simulink model, and are publishing this and all code  
1283 along with the paper. Although most of the components of the model have been published  
1284 before, we believe that this model is the first to incorporate realistic sensorimotor latencies,  
1285 non-zero rest focus, noise *and* dual control by fast and slow integrators, as well as our novel  
1286 use of a non-predictive proportional-control signal. Accordingly, it is able to account well for  
1287 a wide range of empirical observations: the gain and phase of the response to sinusoidal  
1288 oscillations in demand, including the puzzling high-frequency low-frequency resonance; the  
1289 power spectrum of microfluctuations in closed-loop and open-loop modes, and the adaptation  
1290 of accommodation to a steady stimulus.

1291

1292 In our model, accommodation is controlled by four separate signals (Figure 11), which offer  
1293 different benefits. The constant bias signal sets the rest focus, to which the system returns in  
1294 the absence of other stimulation (Figure 18). This may represent a typical demand, making it  
1295 easier for the system to respond when stimulation restarts. The slow integrator means that the

1296 system tends to adapt to steady demand, perhaps reducing disruption if vision is briefly  
1297 interrupted during sustained attention to one distance.

1298

1299 The fast integrator is the main workhorse of the feedback loop, enabling accommodation to  
1300 respond rapidly yet smoothly to changes in demand (Figure 12, Figure 21). It is embedded  
1301 within a predictive control system, incorporating a forward model to predict the effect of  
1302 signals previously sent to the plant. This predictive control enables a smooth response and  
1303 avoids ringing and instability. In principle, it can entirely remove delay due to the sensorimotor  
1304 latency in a situation where demand can be predicted perfectly, as in a regular oscillation.  
1305 However, it becomes problematic where demand changes suddenly and unpredictably.

1306

1307 The fourth signal, proportional to the current defocus, can facilitate rapid responses in such  
1308 situations (Figure 17). Clipping it at a low absolute value ensures that it does not cause  
1309 disastrous oscillations in response. Yet its limited instability in closed-loop generates a periodic  
1310 structure to microfluctuations (Figure 16), which may assist the system in hunting for the point  
1311 of clearest vision. The benefit of having this periodic structure in closed-loop but not open-  
1312 loop mode may be because open-loop viewing occurs naturally for bright viewing conditions,  
1313 where the pupil stops down and depth of focus is large. Microfluctuations due to noise  
1314 resonances would then be of no assistance in improving vision, and might even cause ocular  
1315 fatigue. Presumably for this reason, the system has evolved to select control parameters that  
1316 avoid resonances in open-loop viewing.

1317

1318 “Prediction” in the accommodation literature has often concentrated on predicting changes in  
1319 demand (Krishnan et al., 1973; Stark, 1968). We believe it is helpful to draw a clear distinction  
1320 between predicting one’s own accommodation, which is in principle possible perfectly with an  
1321 efferent copy and a forward model, and predicting demand, which is external and thus not  
1322 always possible, for example when a fixated object moves suddenly. Predicting  
1323 accommodation but simply using the current demand suffices to achieve closed-loop stability.  
1324 The additional benefit of predicting future demand accurately is to avoid delay and thus avoid  
1325 errors for rapidly changing stimuli. However, the low-pass characteristics of the plant and  
1326 leaky-integral controller mean that the benefits of demand prediction are limited unless one  
1327 also posits a different form of control.

1328

1329 The model as currently implemented has many omissions. First, we have not attempted a  
1330 realistic implementation of the demand-prediction model. There is some evidence that the brain  
1331 can predict changing accommodative demand some time into the future, but we have here  
1332 assumed it simply assumes demand will stay constant (Khosroyani & Hung, 2002). Second,  
1333 the model developed here cannot account for the dynamics of step changes, since it does not  
1334 include the “pulse” signal triggered by large step changes in accommodation (Schor &  
1335 Bharadwaj, 2006, 2004), which temporarily overrides the error-driven signal. This of course  
1336 means that the model presented here cannot accurately model the dynamics of the  
1337 accommodative response to such changes. However, the model should remain valid for  
1338 situations which do not trigger a pulse (all the situations modelled in the Results, except Figure  
1339 17BD, included for illustrative purposes). Third, this paper is purely about motor control, and  
1340 has nothing to say about how a signed estimate of defocus is obtained from the retinal image.  
1341 Fourth, we do not allow for physical limits on accommodation, a non-zero far point or  
1342 refractive error, nor do we consider how the system parameters may change with age  
1343 (Bharadwaj & Schor, 2005; Schor & Bharadwaj, 2005). Fifth, we do not consider control  
1344 signals driven by inputs other than retinal defocus and bias (Heath, 1956b; Maddox, 1893).  
1345 Notably, we do not include the crosslinks from and to the vergence system (Bharadwaj, 2005;  
1346 Schor & Kotulak, 1986). We also do not consider other noise sources, such as heartbeat. We  
1347 hope to address these deficiencies in future work.

1348

1349

1350

### 1351 [Financial disclosure and competing interests](#)

1352 This work was part-funded by Magic Leap Inc. by a consultancy contract to Newcastle  
1353 University for the work of JCAR and CKR. Authors BV and BW are employees of Magic Leap  
1354 who initiated the study, reviewed the models and assisted with the preparation of the  
1355 manuscript.

1356



1357  
1358

## Tables

Symbol	Meaning
$\omega$	Angular temporal frequency, $\omega = 2\pi f$
$\phi(f)$	phase-delay of accommodation at frequency $f$
$\tau_{\text{fast}}$	Time-constant of the fast leaky-integrator controller, see Equation 12
$\tau_{\text{plant}}$	Time-constant of the ocular plant, when this is modelled as a leaky integrator, see Equation 11
$\tau_{\text{slow}}$	Time-constant of the slow leaky-integrator controller, see Equation 14
$\zeta$	Damping coefficient, see Equation 22
$\hat{a}(t + T_{\text{mot}})$	Predicted accommodation at a time $T_{\text{mot}}$ after the current time $t$ . In this paper, generally assumed equal to $a(t+T_{\text{mot}})$ , i.e. prediction is perfect.
$\hat{d}(t + T_{\text{mot}})$	Predicted demand at a time $T_{\text{mot}}$ after the current time $t$ . In the no-change prediction model, this is assumed to be the same as the last available demand, from time $T_{\text{sens}}$ before the current time, i.e. $d(t-T_{\text{sens}})$
$A(s)$	Laplace transform of accommodation relative to rest focus
$a_{\text{RF}}$	Rest focus, i.e. accommodation adopted in the absence of any visual stimulus
$a_{\text{SS}}$	Steady-state accommodation in response to $d_{\text{SS}}$ , see Equation 6
$C(s)$	Transfer function of controller
$D(s)$	Laplace transform of accommodative demand relative to rest focus
$d_{\text{SS}}$	Steady-state demand, see Equation 6
$E(s)$	Laplace transform of defocus error, $E(s)=D(s)-A(s)$
$f$	Temporal frequency
$g(f)$	gain of accommodation at frequency $f$
$G_{\text{fast}}$	Steady-state gain of the fast leaky-integrator controller, see Equation 12
$G_{\text{open}}$	steady-state open-loop gain of accommodation

$G_{\text{slow}}$	Steady-state gain of the slow leaky-integrator controller, see Equation 14
$H_{\text{closed}}(s)$	Closed-loop transfer function relating demand to accommodation, see Equation 4
$H_{\text{open}}(s)$	Open-loop transfer function relating demand to accommodation, see Equation 3
$j$	Square root of -1.
$P(s)$	Transfer function of ocular plant
$s$	Complex temporal frequency in Laplace domain, $s = j\omega$ , see Equation 1
$t$	Time
$T_{\text{lat}}$	Total sensorimotor latency, $T_{\text{lat}} = T_{\text{sens}} + T_{\text{mot}}$
$T_{\text{mot}}$	Motor latency, i.e. time taken for the neural signal controlling accommodation to travel from the brain to the ocular plant
$T_{\text{sens}}$	Sensory latency, i.e. time taken for defocus at the retina to reach the accommodative control system in the brain

1359 *Table 1. Symbols used in this paper.*

1360

1361

1362

Parameter	Symbol used in the paper	Name in Simulink workspace	Value
Rest focus	$a_{RF}$	RestFocus	1.4D
Sensory latency	$T_{sens}$	SensoryLatency	0.20s
Motor latency	$T_{mot}$	MotorLatency	0.10s
Time constant of plant	$\tau_{plant}$	PlantTimeConstant	0.156s
Gain of fast integrator	$G_{fast}$	FastGain	8.0
Time constant of fast integrator	$\tau_{fast}$	FastTimeConstant	2.5s
Gain of slow integrator	$G_{slow}$	SlowGain	5.0
Time constant of slow integrator	$\tau_{slow}$	SlowTimeConstant	100s
Noise power		NoisePower	0.001 with sample time 0.01s
Where to clip the proportional signal		ProportionalClipping	0.15D

1363 *Table 2. Parameter values for the Simulink model supplied with the paper and used to obtain the results (except where noted*  
 1364 *otherwise in figure legends). These values are visible in the Simulink Model Workspace, and can be altered there if desired.*

1365

1366

1367

1368

1369

## 1370 Appendix

1371 Here, we derive the total transfer function corresponding to the three types of linear models  
 1372 discussed in the text: (i) the non-predictive model and the predictive models with (ii) perfect  
 1373 and (iii) no-change prediction of demand. The bias signal due to the rest focus  $a_{RF}$  is included  
 1374 as an inhomogeneous “forcing” term. We handle this by defining  $A(s)$  and  $D(s)$  to be the  
 1375 Laplace transforms of  $a(t)-a_{RF}$  and  $d(t)-a_{RF}$ , respectively, where  $a(t)$  and  $d(t)$  are  
 1376 accommodation and demand as functions of time. In this way, we can effectively ignore  $a_{RF}$   
 1377 when obtaining the transfer functions.

1378

### 1379 (i) Non-predictive model

1380 The system diagram for this model is given in Figure 5. Reading around this circuit diagram,  
 1381 we see immediately that

$$1382 \quad E(s) = D(s) - A(s),$$

1383 where  $E(s)$  is the Laplace transform of the defocus error signal,  $d(t)-a(t)$ . The input to the  
 1384 Controller block is  $E(s) \exp(-sT_{sens})$ , i.e. the defocus error signal after the sensory latency.  
 1385 The output from the Controller block is  $C(s)E(s) \exp(-sT_{sens})$ , where  $C(s)$  is the transfer  
 1386 function of the Controller. After accounting for the motor latency, the input to the ocular plant  
 1387 is  $C(s)E(s) \exp(-sT_{lat})$ . So, the output of the ocular plant, i.e. accommodation, is

$$1388 \quad A(s) = H_{plant}(s)C(s)E(s) \exp(-sT_{lat})$$

1389 Substituting in for  $E(s)$ , we obtain the closed-loop transfer function

$$1390 \quad H_{closed}^{classic}(s) = \frac{A(s)}{D(s)} = \frac{P(s)C(s) \exp(-sT_{lat})}{1 + P(s)C(s) \exp(-sT_{lat})}$$

1391 The gain and phase of the accommodative response to sinusoidal stimuli are the amplitude and  
 1392 phase of the complex number given by this closed-loop transfer function evaluated at  
 1393  $s=j\omega=2\pi jf$ ,  $H_{closed}(2\pi jf)$ . The closed-loop gain as a function of demand frequency is  
 1394 therefore

$$1395 \quad G_{closed}^{classic}(f) = \frac{|PC|}{\sqrt{1 + 2Re(PCe^{-2\pi jfT_{lat}}) + |PC|^2}}$$

1396

Equation 17

1397 where the plant and controller transfer functions are similarly complex functions of frequency:  
 1398  $P=P(2\pi jf)$ ,  $C=C(2\pi jf)$ . The denominator contains oscillatory terms which mean that, even if  
 1399  $PC$  is lowpass (i.e. a monotonically decreasing function of frequency), the denominator can be  
 1400 close to zero at particular frequencies and thus produce large resonances, for which the closed-

1401 loop gain exceeds 1. These manifest themselves as ringing or instability in the response to step  
1402 changes in demand, and as gains > 1 for sinusoidal oscillations in demand, which are not  
1403 observed for large amplitudes.

1404

1405 With proportional control with unit gain ( $C=1$ ), a sensorimotor latency of  $T_{lat}=0.3s$  and the  
1406 plant being a leaky integrator with  $\tau_{plant}=0.156s$ , Equation 17 has its first resonance at 1.2Hz  
1407 where the closed-loop gain goes well above 1. This is ultimately responsible for the model's  
1408 high-frequency peak in microfluctuations (Figure 16) and the low-amplitude resonance in the  
1409 response to sine-waves (Figure 13), although the precise behaviour also depends on the  
1410 nonlinear clipping. The precise position of the first resonance depends on the gain of the  
1411 proportional control, but only rather subtly. We therefore kept unit gain for simplicity.

1412 We obtain the open-loop transfer function in the same way, but with the input to the Controller  
1413 being  $D(s)$  instead of  $D(s)-A(s)$ . This yields

$$1414 \quad H_{open}^{classic}(s) = P(s)C(s) \exp(-sT_{lat})$$

$$1415 \quad G_{open}^{classic}(\omega) = |PC|$$

1416

*Equation 18*

1417 Thus, whether we use an integral or proportional controller in this non-predictive control  
1418 system, the open-loop gain is purely low-pass, with no resonances. This means that adding our  
1419 non-predictive proportional signal does not introduce any peaks to the power spectrum of open-  
1420 loop microfluctuations.

1421

## 1422 Predictive models

1423 The simplified system diagram for this model is given in Figure 7. As usual, we can ignore the  
1424 bias signal if we express accommodation and demand relative to the rest focus. Reading around  
1425 the circuit diagram, the demand signal is the input on the left; we represent this as usual in the  
1426 Laplace domain by  $D(s)$ . After passing through the sensory latency, it becomes  
1427  $D(s) \exp(-sT_{sens})$ , with the exponential being the Laplacian representation of a time delay  
1428 (cf discussion of Equation 2). It then passes through the demand predictor, which attempts to  
1429 predict the signal  $T_{lat} = T_{sens} + T_{mot}$  into the future. If it did this perfectly, the output of the demand  
1430 predictor would be  $D(s) \exp(-sT_{sens}) \exp(-sT_{lat}) = D(s) \exp(+sT_{mot})$ . To allow for the  
1431 fact that demand is unlikely to be predicted perfectly, we will write the output as  
1432  $\hat{D}(s) \exp(+sT_{mot})$ .  $\hat{D}(s)$  is the Laplace transform of the estimated future demand, again

1433 relative to the rest focus. That is, whereas  $d(t)$  is the actual demand at time  $t$ ,  $\hat{d}(t)$  is the  
 1434 estimated demand at time  $t$ , as estimated at time  $(t-T_{lat})$ .

1435 Looking at the bottom of Figure 7, the output is accommodation, or  $A(s)$  in the Laplace domain.  
 1436 This is output after a motor latency  $T_{mot}$ ; thus the output of the “Plant” block in Figure 7 is  
 1437  $A(s) \exp(+sT_{mot})$ .

1438 Putting both these together, we see that the input to the Controller in Figure 7 is  
 1439  $[\hat{D}(s) - A(s)] \exp(+sT_{mot})$ . After multiplying this by the Controller and Plant transfer  
 1440 functions, we find that the output of the plant is  $P(s)C(s)[\hat{D}(s) - A(s)] \exp(+sT_{mot})$ . But we  
 1441 previously saw that the output of the plant is  $A(s) \exp(+sT_{mot})$ . Equating these, we see that

$$1442 \quad A(s) = P(s)C(s)[\hat{D}(s) - A(s)]$$

1443 and thus that

$$1444 \quad A(s) = \frac{P(s)C(s)\hat{D}(s)}{1 + P(s)C(s)}$$

1445 Equation 19

1446

1447 (ii) Perfect demand predictor

1448 In this idealised case, the demand predictor successfully outputs the future accommodative  
 1449 demand, so that  $\hat{D}(s) = D(s)$  and the transfer function is

$$1450 \quad H_{closed}^{perfect}(s) = \frac{P(s)C(s)}{1 + P(s)C(s)}$$

1451 The closed-loop gain is therefore

$$1452 \quad g_{closed}^{perfect}(f) = \frac{|PC|}{\sqrt{1 + 2Re(PC) + |PC|^2}}$$

1453 To obtain the open-loop transfer function, we replace  $D(s)$  with  $D(s)+A(s)$  in Equation 19  
 1454 (Figure 4), obtaining

$$1455 \quad A(s) = \frac{P(s)C(s)[A(s) + D(s)]}{1 + P(s)C(s)}$$

1456 and thus

$$1457 \quad H_{open}^{perfect}(s) = P(s)C(s)$$

1458 If demand prediction is perfect, the open-loop gain of the controller is independent of latency.

1459 For our situation where both the plant and controller are leaky integrators, the open-loop gain  
 1460 is lowpass, with no resonances.

1461

1462 (iii) “No-change” demand predictor

1463 In this opposite extreme, the demand predictor simply assumes that the future defocus after  
1464 time  $T_{lat}$  will still be the same as the defocus it is receiving now (Equation 9):

$$1465 \quad \hat{d}(t + T_{lat}) = d(t)$$

1466 and thus

$$1467 \quad \hat{D}(s) = D(s)\exp(-sT_{lat})$$

1468 Hence

$$1469 \quad H_{closed}^{nochange}(s) = \frac{P(s)C(s)\exp(-sT_{lat})}{1 + P(s)C(s)}$$

1470 The closed-loop gain at any frequency  $f$  is therefore the same as for the perfect predictor, while  
1471 the phase is reduced by  $2\pi fT_{lat}$ . In fact, the closed-loop gain would be the same for any demand  
1472 predictor which accurately predicts demand any time at all into the future, even if, as here, that  
1473 time is zero. Inaccurate predictions would of course change the closed-loop gain.

1474

1475 The open-loop gain does depend critically on demand prediction. With no-change prediction,  
1476 replacing  $D(s)$  with  $D(s)+A(s)$  in Equation 19 (Figure 4), yields

$$1477 \quad A(s) = \frac{P(s)C(s)[A(s) + D(s)]\exp(-sT_{lat})}{1 + P(s)C(s)}$$

1478 and thus

$$1479 \quad H_{open}^{nochange}(s) = \frac{P(s)C(s)\exp(-sT_{lat})}{1 + P(s)C(s)(1 - \exp(-sT_{lat}))}$$

1480

Equation 20

1481 The presence of the oscillatory  $\exp(-sT_{lat})$  term in the denominator can lead to local peaks in  
1482 the gain at some frequencies. Thus with inaccurate no-change prediction, the system is prone  
1483 to open-loop resonances due to the inner feedback loop via the efference copy. However, with  
1484 our parameter values (Table 2), Equation 20 is a monotonically decreasing function of  
1485 frequency. This ensures that we do not see local peaks in the power spectrum of open-loop  
1486 microfluctuations (Figure 16).

1487

1488

1489 [The predictive model with leaky-integral control: a damped harmonic oscillator](#)

1490 For the case where the plant and the controller are both leaky integrators (Equation 11, Equation

1491 12), and we neglect the other signals, the transfer function of the perfect-prediction model is

1492 
$$H_{closed}^{perfect}(s) = \frac{G_{fast}}{(1 + s\tau_{plant})(1 + s\tau_{fast}) + G_{fast}}$$

1493 Equation 21

1494 with  $s = 2\pi jf$ . This is the transfer function of a second-order damped oscillator. We can rewrite  
1495 it in the standard form

1496 
$$H_{closed}^{perfect}(s) \approx \frac{K\omega_0^2}{s^2 + 2\zeta\omega_0s + \omega_0^2}$$

1497 where K is the closed-loop gain:

1498 
$$K = \frac{G_{fast}}{(1 + G_{fast})}$$

1499  $\omega_0$  the natural angular frequency:

1500 
$$\omega_0^2 = \frac{(1 + G_{fast})}{\tau_{plant}\tau_{fast}}$$

1501 and  $\zeta$  the damping coefficient:

1502 
$$\zeta = \frac{1}{2\sqrt{1 + G_{fast}}} \frac{(\tau_{plant} + \tau_{fast})}{\sqrt{\tau_{plant}\tau_{fast}}}$$

1503 Equation 22

1504 For perfect demand prediction, the phase at angular frequency  $\omega$  is:

1505 
$$\phi^{perfect}(\omega) = -\arctan\left(\frac{2\zeta\omega\omega_0}{\omega_0^2 - \omega^2}\right)$$

1506 while for no-change prediction,

1507 
$$\phi^{nochange}(\omega) = -\arctan\left(\frac{2\zeta\omega\omega_0}{\omega_0^2 - \omega^2}\right) - \omega T_{lat}$$

1508

1509 If  $\zeta < 1/\sqrt{2}$ , then the maximum gain occurs at the resonant angular frequency:

1510 
$$\omega_{res} = \omega_0\sqrt{1 - 2\zeta^2} = \sqrt{\frac{G_{fast}}{\tau_{plant}\tau_{fast}} - \frac{1}{2\tau_{fast}^2} - \frac{1}{2\tau_{plant}^2}}$$

1511 If  $\zeta > 1/\sqrt{2}$ , then the gain is maximum for  $f=0$  and decreases monotonically with frequency. If  
1512  $\zeta=1$ , the system is said to be critically damped.

1513 As discussed in the text, to match the empirical gain of accommodation,  $\zeta$  must exceed  $1/\sqrt{2}$ ,  
1514 the minimum value for which gain decreases monotonically with frequency. Solving Equation  
1515 22, we find that



1516  $\tau_{fast} = \tau_{plant} \left( G_{fast} + \sqrt{G_{fast}^2 - 1} \right) \approx 2G_{fast}\tau_{plant}$  yields  $\zeta = 1/\sqrt{2}$ , while

1517  $\tau_{fast} = \tau_{plant} \left( 2G_{fast} + 1 + \sqrt{[2G_{fast} + 1]^2 - 1} \right) \approx 4G_{fast}\tau_{plant}$  yields  $\zeta=1$ , i.e. critical

1518 damping

1519

1520 where the approximations hold since the gain  $G_{fast}$  has to be  $\gg 1$ , say at least 5, to avoid  
1521 excessive lag. (Mathematically, there are two solutions, but the other one gives a very short  
1522 time-constant for the controller, which in turn causes other problems such as open-loop  
1523 resonances in the noise.)

1524

1525 The minimal-settling time solution

1526 In the model presented here, we chose the “minimum settling time” solution which yields  $\zeta =$   
1527  $1/\sqrt{2}$ :

1528 
$$\tau_{fast} = 2G_{fast}\tau_{plant}$$

1529 since this gave the best match to both gain and phase data. With this choice, since  $G_{fast} \gg 1$ , the  
1530 natural frequency is approximately

1531 
$$\omega_0 = \frac{1}{\tau_{plant}\sqrt{2}}$$

1532 which with our value  $\tau_{plant}=0.156s$  corresponds to 0.72Hz.

1533 For  $\zeta=1/\sqrt{2}$ , the phase function is very close to linear out to  $\omega=\omega_0$ . In this region, for perfect  
1534 demand prediction

1535 
$$\phi^{perfect} \approx -2\tau_{plant}\omega$$

1536 corresponding to an effective delay of  $T_{delay} = 2\tau_{plant}$ . Presumably coincidentally, this delay is  
1537 very similar to the sensorimotor latency, although as we can see it arises from a completely  
1538 different source. However, for frequencies beyond  $\sim 1Hz$ , the phase asymptotes to  $180^\circ$  (Figure  
1539 8).

1540 For no-change prediction, the phase is approximately

1541 
$$\phi(\omega) \approx -\omega(2\tau_{plant} + T_{lat})$$

1542 at low frequencies, corresponding to an effective delay of  $2\tau_{plant} + T_{lat}$ .

1543

1544

1545

1546

Transfer function $A(s)$ $= H(s)D(s)$	Non-predictive model – no prediction	Predictive model – perfect prediction of future demand	Predictive model – “no change” prediction of future demand
Open-loop transfer function	$PCe^{-sT_{lat}}$	$PC$	$\frac{PCe^{-sT_{lat}}}{1 + PC(1 - e^{-sT_{lat}})}$
Closed-loop transfer function	$\frac{PCe^{-sT_{lat}}}{1 + PCe^{-sT_{lat}}}$	$\frac{PC}{1 + PC}$	$\frac{PCe^{-sT_{lat}}}{1 + PC}$
Closed-loop gain	$\frac{ PC }{\sqrt{1 + 2Re(PCe^{-i\omega T_{lat}}) +  PC ^2}}$	$\frac{ PC }{\sqrt{1 + 2Re(PC) +  PC ^2}}$	$\frac{ PC }{\sqrt{1 + 2Re(PC) +  PC ^2}}$

1547 Table 3. Open- and closed-loop transfer functions  $H(s)$  for different control systems; see Appendix for derivation. The transfer  
 1548 function relates accommodation to the demand via  $A(s) = H(s) D(s)$ , where  $A(s)$  is the Laplace transform of accommodation  
 1549 relative to rest focus,  $a(t)-a_{RF}$ , and  $D(s)$  is the Laplace transform of demand relative to rest focus,  $d(t)-a_{RF}$ .  $P(s)$  the transfer  
 1550 function of the ocular plant, and  $C(s)$  is the transfer function of the neural control (block marked Controller in Figure 5, Figure  
 1551 6, Figure 7).  $T_{lat}$  is the total sensorimotor latency from a change in demand to the accommodative response.

1552

## 1553 References

- 1554 Águila-Carrasco, A. J. D., & Marín-Franch, I. (2021). Predictability of sinusoidally moving stimuli does  
 1555 not improve the accuracy of the accommodative response. *Scientific Reports*, *11*(1), 15195.  
 1556 <https://doi.org/10.1038/s41598-021-94642-2>
- 1557 Bahill, A. T., Clark, M. R., & Stark, L. (1975). Computer simulation of overshoot in saccadic eye  
 1558 movements. *Computer Programs in Biomedicine*, *4*(4), 230–236.  
 1559 [https://doi.org/10.1016/0010-468X\(75\)90036-7](https://doi.org/10.1016/0010-468X(75)90036-7)

- 1560 Beers, A. P. A., & Van Der Heijde, G. L. (1994). In vivo determination of the biomechanical properties  
1561 of the component elements of the accommodation mechanism. *Vision Research*, 34(21),  
1562 2897–2905. [https://doi.org/10.1016/0042-6989\(94\)90058-2](https://doi.org/10.1016/0042-6989(94)90058-2)
- 1563 Beers, A. P., & van der Heijde, G. L. (1996). Age-related changes in the accommodation mechanism.  
1564 *Optometry and Vision Science : Official Publication of the American Academy of Optometry*,  
1565 73(4), 235–242. <https://doi.org/10.1097/00006324-199604000-00004>
- 1566 Bharadwaj, S. R. (2005). *Neural Control Strategies of the Human Focusing Mechanism*.
- 1567 Bharadwaj, S. R., & Schor, C. M. (2005). Acceleration characteristics of human ocular accommodation.  
1568 *Vision Research*, 45(1), 17–28. <https://doi.org/10.1016/j.visres.2004.07.040>
- 1569 Bharadwaj, S. R., & Schor, C. M. (2006). Dynamic control of ocular disaccommodation: First and  
1570 second-order dynamics. *Vision Res*, 46(6–7). <https://doi.org/10.1016/j.visres.2005.06.005>
- 1571 Burge, J., & Geisler, W. S. (2011). Optimal defocus estimation in individual natural images. *Proc Natl*  
1572 *Acad Sci U S A*, 108(40), 16849–16854. <https://doi.org/1108491108> [pii]  
1573 10.1073/pnas.1108491108
- 1574 Campbell, F. W., Robson, J. G., & Westheimer, G. (1959a). Fluctuations of accommodation under  
1575 steady viewing conditions. *The Journal of Physiology*, 145(3), 579–594.  
1576 <https://doi.org/10.1113/jphysiol.1959.sp006164>
- 1577 Campbell, F. W., Robson, J. G., & Westheimer, G. (1959b). Fluctuations of accommodation under  
1578 steady viewing conditions. *The Journal of Physiology*, 145(3), 579–594.  
1579 <https://doi.org/10.1113/jphysiol.1959.sp006164>
- 1580 Campbell, F. W., & Westheimer, G. (1960). Dynamics of accommodation responses of the human eye.  
1581 *The Journal of Physiology*, 151(2), 285–295. <https://doi.org/10.1113/jphysiol.1960.sp006438>
- 1582 Charman, W. N., & Heron, G. (1988). Fluctuations in accommodation: A review. *Ophthalmic &*  
1583 *Physiological Optics: The Journal of the British College of Ophthalmic Opticians (Optometrists)*,  
1584 8(2), 153–164. <https://doi.org/10.1111/j.1475-1313.1988.tb01031.x>

- 1585 Charman, W. N., & Heron, G. (2000). On the linearity of accommodation dynamics. *Vision Research*,  
1586 40(15), 2057–2066. [https://doi.org/10.1016/S0042-6989\(00\)00066-3](https://doi.org/10.1016/S0042-6989(00)00066-3)
- 1587 Charman, W. N., & Heron, G. (2015). Microfluctuations in accommodation: An update on their  
1588 characteristics and possible role. *Ophthalmic and Physiological Optics*, 35(5), 476–499.  
1589 <https://doi.org/10.1111/opo.12234>
- 1590 Cholewiak, S. A., Love, G. D., & Banks, M. S. (2018). Creating correct blur and its effect on  
1591 accommodation. *Journal of Vision*, 18(9). <https://doi.org/10.1167/18.9.1>
- 1592 Collins, M., Davis, B., & Wood, J. (1995). Microfluctuations of steady-state accommodation and the  
1593 cardiopulmonary system. *Vision Research*, 35(17), 2491–2502.
- 1594 Denieul, P. (1982). Effects of stimulus vergence on mean accommodation response, microfluctuations  
1595 of accommodation and optical quality of the human eye. *Vision Research*, 22(5), 561–569.  
1596 [https://doi.org/10.1016/0042-6989\(82\)90114-6](https://doi.org/10.1016/0042-6989(82)90114-6)
- 1597 Ejiri, M., Thompson, H. E., & O'Neill, W. D. (1969). Dynamic visco-elastic properties of the lens. *Vision*  
1598 *Research*, 9(2), 233–244. [https://doi.org/10.1016/0042-6989\(69\)90003-0](https://doi.org/10.1016/0042-6989(69)90003-0)
- 1599 Fincham, E. F. (1951). The Accommodation Reflex and its Stimulus. *The British Journal of*  
1600 *Ophthalmology*, 35(7), 381–393.
- 1601 Gall, J. (1977). *Systemantics: How Systems Work & Especially How They Fail*. Times Books.
- 1602 Gamba, E., Sawides, L., Dorransoro, C., & Marcos, S. (2009). Accommodative lag and fluctuations  
1603 when optical aberrations are manipulated. *Journal of Vision*, 9(6), 4.1-15.  
1604 <https://doi.org/10.1167/9.6.4>
- 1605 Gamlin, P. D., Zhang, Y., Clendaniel, R. A., & Mays, L. E. (1994). Behavior of identified Edinger-Westphal  
1606 neurons during ocular accommodation. *Journal of Neurophysiology*, 72(5), 2368–2382.  
1607 <https://doi.org/10.1152/jn.1994.72.5.2368>
- 1608 Gray, L. S., Winn, B., & Gilmartin, B. (1993a). Effect of target luminance on microfluctuations of  
1609 accommodation. *Ophthalmic & Physiological Optics: The Journal of the British College of*

- 1610            *Ophthalmic Opticians (Optometrists)*, 13(3), 258–265. <https://doi.org/10.1111/j.1475->  
1611            1313.1993.tb00468.x
- 1612    Gray, L. S., Winn, B., & Gilmartin, B. (1993b). Accommodative microfluctuations and pupil diameter.  
1613            *Vision Research*, 33(15), 2083–2090. [https://doi.org/10.1016/0042-6989\(93\)90007-j](https://doi.org/10.1016/0042-6989(93)90007-j)
- 1614    Heath, G. G. (1956a). The influence of visual acuity on accommodative responses of the eye. *American*  
1615            *Journal of Optometry and Archives of American Academy of Optometry*, 33(10), 513–524.  
1616            <https://doi.org/10.1097/00006324-195610000-00001>
- 1617    Heath, G. G. (1956b). Components of accommodation. *American Journal of Optometry and Archives*  
1618            *of American Academy of Optometry*, 33(11), 569–579. <https://doi.org/10.1097/00006324->  
1619            195611000-00001
- 1620    Heron, G., Charman, W. N., & Gray, L. S. (1999). Accommodation Responses and Ageing. *Investigative*  
1621            *Ophthalmology & Visual Science*, 40(12), 2872–2883.
- 1622    Hung, G. K., Ciuffreda, K. J., Khosroyani, M., & Jiang, B.-C. (2002). *Models of Accommodation* (pp. 287–  
1623            339). [https://doi.org/10.1007/978-1-4757-5865-8\\_8](https://doi.org/10.1007/978-1-4757-5865-8_8)
- 1624    Khosroyani, M., & Hung, G. K. (2002). A Dual-Mode Dynamic Model of the Human Accommodation  
1625            System. *Bulletin of Mathematical Biology*, 64(2), 285–299.  
1626            <https://doi.org/10.1006/bulm.2001.0274>
- 1627    Kotulak, J. C., & Schor, C. M. (1986a). The accommodative response to subthreshold blur and to  
1628            perceptual fading during the Troxler phenomenon. *Perception*, 15(1), 7–15.  
1629            <https://doi.org/10.1068/p150007>
- 1630    Kotulak, J. C., & Schor, C. M. (1986b). Temporal variations in accommodation during steady-state  
1631            conditions. *Journal of the Optical Society of America. A, Optics and Image Science*, 3(2), 223–  
1632            227. <https://doi.org/10.1364/josaa.3.000223>
- 1633    Kotulak, J. C., & Schor, C. M. (1986c). A computational model of the error detector of human visual  
1634            accommodation. *Biological Cybernetics*, 54(3), 189–194.  
1635            <https://doi.org/10.1007/BF00356857>

- 1636 Krishnan, V. V., Phillips, S., & Stark, L. (1973). Frequency analysis of accommodation, accommodative  
1637 vergence and disparity vergence. *Vision Research*, *13*(8), 1545–1554.
- 1638 Krishnan, V. V., & Stark, L. (1975). Integral control in accommodation. *Computer Programs in*  
1639 *Biomedicine*, *4*(4), 237–245. [https://doi.org/10.1016/0010-468X\(75\)90037-9](https://doi.org/10.1016/0010-468X(75)90037-9)
- 1640 Kruger, P. B., Mathews, S., Aggarwala, K. R., & Sanchez, N. (1993). Chromatic aberration and ocular  
1641 focus: Fincham revisited. *Vision Research*, *33*(10), 1397–1411. [https://doi.org/10.1016/0042-](https://doi.org/10.1016/0042-6989(93)90046-y)  
1642 [6989\(93\)90046-y](https://doi.org/10.1016/0042-6989(93)90046-y)
- 1643 Kruger, P. B., & Pola, J. (1986). Stimuli for accommodation: Blur, chromatic aberration and size. *Vision*  
1644 *Research*, *26*(6), 957–971. [https://doi.org/10.1016/0042-6989\(86\)90153-7](https://doi.org/10.1016/0042-6989(86)90153-7)
- 1645 Labhishetty, V., & Bobier, W. R. (2017). Are high lags of accommodation in myopic children due to  
1646 motor deficits? *Vision Research*, *130*, 9–21. <https://doi.org/10.1016/j.visres.2016.11.001>
- 1647 Leibowitz, H. W., & Owens, D. A. (1978). New evidence for the intermediate position of relaxed  
1648 accommodation. *Documenta Ophthalmologica. Advances in Ophthalmology*, *46*(1), 133–147.  
1649 <https://doi.org/10.1007/BF00174103>
- 1650 Maddox, E. E. (1893). *The Clinical Use of Prisms; and the Decentering of Lenses, 2nd edition*. John  
1651 *Wright & Sons, Bristol, England*. (2nd ed.). John Wright & Sons.
- 1652 Miall, R. C., Weir, D. J., Wolpert, D. M., & Stein, J. (1993). Is the cerebellum a Smith predictor? *Journal*  
1653 *of Motor Behaviour*, *25*(3), 203–216.
- 1654 Ohtsuka, K., & Sawa, M. (1997). Frequency characteristics of accommodation in a patient with  
1655 agenesis of the posterior vermis and normal subjects. *British Journal of Ophthalmology*, *81*(6),  
1656 476–480. <https://doi.org/10.1136/bjo.81.6.476>
- 1657 Otero, C., Aldaba, M., Díaz-Doutón, F., Vera-Díaz, F. A., & Pujol, J. (2019). Stimulus Unpredictability in  
1658 Time, Magnitude, and Direction on Accommodation. *Optometry and Vision Science: Official*  
1659 *Publication of the American Academy of Optometry*, *96*(6), 424–433.  
1660 <https://doi.org/10.1097/OPX.0000000000001384>

- 1661 Phillips, S., Shirachi, D., & Stark, L. (1972). ANALYSIS OF ACCOMMODATIVE RESPONSE TIMES USING  
1662 HISTOGRAM INFORMATION. *American Journal of Optometry and Archives of American*  
1663 *Academy of Optometry*, 49(5), 389–400.
- 1664 Popa, L. S., & Ebner, T. J. (2019). Cerebellum, Predictions and Errors. *Frontiers in Cellular Neuroscience*,  
1665 12. <https://doi.org/10.3389/fncel.2018.00524>
- 1666 Rosenfield, M., Ciuffreda, K. J., Hung, G. K., & Gilmartin, B. (1993a). Tonic accommodation: A review.  
1667 I. Basic aspects. *Ophthalmic & Physiological Optics : The Journal of the British College of*  
1668 *Ophthalmic Opticians (Optometrists)*, 13(3), 266–284.
- 1669 Rosenfield, M., Ciuffreda, K. J., Hung, G. K., & Gilmartin, B. (1993b). Tonic accommodation: A review.  
1670 I. Basic aspects. *Ophthalmic & Physiological Optics : The Journal of the British College of*  
1671 *Ophthalmic Opticians (Optometrists)*, 13(3), 266–284. <https://doi.org/10.1111/j.1475->  
1672 [1313.1993.tb00469.x](https://doi.org/10.1111/j.1475-1313.1993.tb00469.x)
- 1673 Schor, C. M. (1979a). The influence of rapid prism adaptation upon fixation disparity. *Vision Research*,  
1674 19(7), 757–765. [https://doi.org/10.1016/0042-6989\(79\)90151-2](https://doi.org/10.1016/0042-6989(79)90151-2)
- 1675 Schor, C. M. (1979b). The relationship between fusional vergence eye movements and fixation  
1676 disparity. *Vision Research*, 19(12), 1359–1367. [https://doi.org/10.1016/0042-6989\(79\)90208-](https://doi.org/10.1016/0042-6989(79)90208-)  
1677 6
- 1678 Schor, C. M., & Bharadwaj, S. R. (2005). A pulse-step model of accommodation dynamics in the aging  
1679 eye. *Vision Research*, 45(10), 1237–1254. <https://doi.org/10.1016/j.visres.2004.11.011>
- 1680 Schor, C. M., & Bharadwaj, S. R. (2006). Pulse-step models of control strategies for dynamic ocular  
1681 accommodation and disaccommodation. *Vision Research*, 46(1), 242–258.  
1682 <https://doi.org/10.1016/j.visres.2005.09.030>
- 1683 Schor, C. M., & Bharadwaj, S. R. (2004). A pulse-step model of accommodation dynamics. *The 26th*  
1684 *Annual International Conference of the IEEE Engineering in Medicine and Biology Society*, 3,  
1685 766–769. <https://doi.org/10.1109/IEMBS.2004.1403271>

- 1686 Schor, C. M., & Kotulak, J. C. (1986). Dynamic interactions between accommodation and convergence  
1687 are velocity sensitive. *Vision Research*, 26(6), 927–942. <https://doi.org/10.1016/0042->  
1688 6989(86)90151-3
- 1689 Schor, C. M., Kotulak, J. C., & Tsuetaki, T. (1986). Adaptation of tonic accommodation reduces  
1690 accommodative lag and is masked in darkness. *Investigative Ophthalmology & Visual Science*,  
1691 27(5), 820–827.
- 1692 Schor, C. M., Lott, L. A., Pope, D., & Graham, A. D. (1999). Saccades reduce latency and increase  
1693 velocity of ocular accommodation. *Vision Research*, 39(22), 3769–3795.  
1694 [https://doi.org/10.1016/s0042-6989\(99\)00094-2](https://doi.org/10.1016/s0042-6989(99)00094-2)
- 1695 Seidemann, A., & Schaeffel, F. (2002). Effects of longitudinal chromatic aberration on accommodation  
1696 and emmetropization. *Vision Research*, 42(21), 2409–2417. <https://doi.org/10.1016/S0042->  
1697 6989(02)00262-6
- 1698 Smith, O. (1957). Closer control of loops with dead time. *Chemical Engineering Progress*, 53(5), 217–  
1699 219.
- 1700 Stark, L. (1968). Accommodative Tracking: A Trial-and-Error Function. In L. Stark (Ed.), *Neurological*  
1701 *Control Systems: Studies in Bioengineering* (pp. 220–230). Springer US.  
1702 [https://doi.org/10.1007/978-1-4684-0706-8\\_10](https://doi.org/10.1007/978-1-4684-0706-8_10)
- 1703 Stark, L., Takahashi, Y., & Zames, G. (1965). Nonlinear Servoanalysis of Human Lens Accommodation.  
1704 *IEEE Transactions on Systems Science and Cybernetics*, 1(1), 75–83.  
1705 <https://doi.org/10.1109/TSSC.1965.300064>
- 1706 Sun, F., Brandt, S., Nguyen, A., Wong, M., & Stark, L. (1989). Frequency analysis of accommodation:  
1707 Single sinusoids. *Ophthalmic & Physiological Optics: The Journal of the British College of*  
1708 *Ophthalmic Opticians (Optometrists)*, 9(4), 392–397.
- 1709 Sun, F. C., & Stark, L. (1990). Switching control of accommodation: Experimental and simulation  
1710 responses to ramp inputs. *IEEE Transactions on Bio-Medical Engineering*, 37(1), 73–79.  
1711 <https://doi.org/10.1109/10.43618>



- 1712 Toates, F. M. (1972). Accommodation function of the human eye. *Physiological Reviews*, 52(4).
- 1713 Udlam, W. M., Wittenberg, S., Giglio, E. J., & Rosenberg, R. (1968). Accommodative responses to small  
1714 changes in dioptric stimulus. *American Journal of Optometry and Archives of American*  
1715 *Academy of Optometry*, 45(8), 483–506. [https://doi.org/10.1097/00006324-196808000-](https://doi.org/10.1097/00006324-196808000-00001)  
1716 00001
- 1717 Wildt, G. J. van der, Bouman, M. A., & Kraats, J. van de. (1974). The Effect of Anticipation on the  
1718 Transfer Function of the Human Lens System. *Optica Acta: International Journal of Optics*,  
1719 21(11), 843–860. <https://doi.org/10.1080/713818858>
- 1720 Wilson, B. J., Decker, K. E., & Roorda, A. (2002). Monochromatic aberrations provide an odd-error cue  
1721 to focus direction. *Journal of the Optical Society of America A-Optics Image Science and Vision*,  
1722 19(5), 833–839.
- 1723 Wilson, D. (1973). A centre for accommodative vergence motor control. *Vision Research*, 13(12),  
1724 2491–2503. [https://doi.org/10.1016/0042-6989\(73\)90246-0](https://doi.org/10.1016/0042-6989(73)90246-0)
- 1725 Winn, B., Pugh, J. R., Gilmartin, B., & Owens, H. (1990). Arterial pulse modulates steady-state ocular  
1726 accommodation. *Current Eye Research*, 9(10), 971–975.  
1727 <https://doi.org/10.3109/02713689009069933>
- 1728 Yao, P., Lin, H., Huang, J., Chu, R., & Jiang, B. (2010). Objective depth-of-focus is different from  
1729 subjective depth-of-focus and correlated with accommodative microfluctuations. *Vision*  
1730 *Research*, 50(13), 1266–1273. <https://doi.org/10.1016/j.visres.2010.04.011>
- 1731